Conformation of the Trypanocidal Pharmaceutical Suramin in Its Free and Bound Forms: Transferred Nuclear Overhauser Studies†

Tatyana Polenova,‡ Takashi Iwashita,‡,§ Arthur G. Palmer, III,|| and Ann E. McDermott*,‡

Department of Chemistry and Department of Biochemistry and Molecular Biophysics, Columbia University, New York, New York 10027

Received February 7, 1997; Revised Manuscript Received June 2, 1997⊗

ABSTRACT: Suramin is a lead compound for treatment of cancer, HIV, and trypanosomiasis. The conformations of suramin in its free form and bound to phosphoglycerate kinases from *T. brucei* and *S. cerevisae*, have been studied in aqueous solutions using nuclear Overhauser effect (NOE) and transferred NOE NMR spectroscopies. The NOE data of the free drug can be accommodated by a model in which many of the single bonds of suramin are unrestricted at room temperature, consistent with molecular mechanics calculations. The angle between the naphthalene ring and the adjoining amide is essentially locked by a strong amide−sulfonate hydrogen bond into one preferred conformation. Another degree of freedom near the termini of the molecule has a rather pronounced preference, and a third exhibits a nearly perpendicular arrangement between the amide and adjacent aromatic ring. The other two degrees of freedom have weaker preferences. Molecular mechanics calculations using AMBER force field and charges on amides and sulfonates obtained from semiempirical or *ab initio* calculations reproduced the extent of nonplanarity but not the detailed preferences. ^{13}C spin−lattice relaxation, proton NOE, and light-scattering measurements for free suramin indicate that the correlation time of the molecule is approximately 3 ns at 5 mM concentration, suggesting that suramin is multimeric. Lowering the temperature to 5 °C causes a dramatic broadening of all of the resonances in the NMR spectra of 5 mM suramin. This broadening probably is associated with further aggregation into micelles. Suramin is monomeric at 0.5 mM and room temperature, and the NOE cross-relaxation rate constants are close to the cancellation condition for a 500 MHz proton frequency; this concentration is typical of blood serum concentrations when the drug is utilized in humans. Changes in the conformational preferences for terminal degrees of freedom are observed in the bound states of suramin based upon the transferred NOE data. The data for the bound state cannot be accommodated by a symmetric conformer. Analysis of the transferred NOESY buildup curves indicates complex kinetics of binding, probably involving an electrostatically bound encounter complex. Despite the weak binding constant, the buildup curves cannot be treated as population-weighted averages of the free and bound cross-relaxation rates, and therefore complete relaxation−exchange matrix analysis has been performed to simulate the data sets.

Since the 1920s suramin has been a common treatment for African trypanosomiasis (Willson et al., 1993). Suramin is a large polysulfonated, polyaromatic compound linked by amides (Figure 1). Near the turn of the century, Ehrlich screened many dye compounds and found trypanocidal activity in sulfonated aromatic compounds such as Nagana red (Harte, 1990). Suramin is a more effective analog of Nagana red produced by Bayer in 1916. The synthesis and composition of suramin was first completely described in 1924 (Fourneau et al., 1924). It is still commonly used in a veterinarial as well as a medicinal capacity against *Trypanosoma brucei*. Recently suramin has also been studied as a potential HIV[1] reverse transcriptase inhibitor (Jentsch et al., 1987) and an antineoplastic compound active against prostate cancer, possibly acting by blocking the interactions of the heparin-binding growth factors with their receptors (Stein, 1993).

The trypanocidal action of suramin has been proposed on the basis of *in vivo* data to be inhibition of the parasite low-density lipoproteins (LDL) receptor (Vansterkenburg et al., 1993) followed by inhibition of glycolysis (Fairlamb & Bowman, 1980). Association of suramin with the glycolytic enzymes has been demonstrated (Vansterkenburg et al., 1993). Limited cellular uptake of suramin by both host and parasite has been proposed to occur by the process of receptor-mediated fluid-phase endocytosis, probably mediated by the LDL receptor (Stein, 1993; Vansterkenburg et al., 1993). Suramin is clinically active at approximately 10 μM (minimum effective dosage), which is well below the maximum safe and typically used dosage for humans of

† A.M. and T.P. acknowledge support from the Kanagawa Academy of Science and Technology (KAST) and Columbia University. A.G.P. acknowledges support from the American Cancer Society (JFRA-540) and National Institutes of Health (GM50291).

‡ Department of Chemistry.

§ Department of Biochemistry and Molecular Biophysics.

|| Present address: Suntory Research Institute, Osaka, Japan.

⊗ Abstract published in *Advance ACS Abstracts,* August 1, 1997.

[1] Abbreviations: COSY, correlation spectroscopy; CSA, chemical shift anisotropy; DEPT, distortionless enhanced polarization transfer; HIV, human immunodefficiency virus; HSQC, heteronuclear single quantum coherence (spectroscopy); IPTG, isopropyl β-D-thiogalactopyranoside; LDL, low-density lipoproteins; NOE, nuclear Overhauser effect; NOESY, nuclear Overhauser enhancement spectroscopy; transferred NOESY, transferred nuclear Overhauser enhancement spectroscopy; PGK, phosphoglycerate kinase; ROESY, rotating frame Overhauser enhancement spectroscopy; SAR, structure−activity relationship; T_1, spin−lattice relaxation time constant; T_2, spin−spin relaxation time constant; TIM, triose phosphate isomerase; TPPI, time proportional phase incrementation; WATERGATE, water suppression by gradient tailored excitation.

S0006-2960(97)00297-3 CCC: $14.00

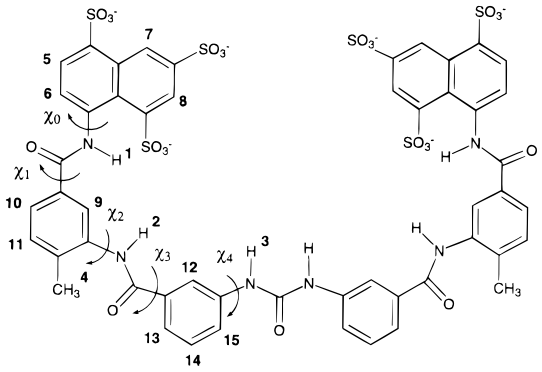

FIGURE 1: Molecular structure of suramin. Possible degrees of conformational freedom and the corresponding dihedral angles $\chi_1-\chi_4$ are shown using arrows.

approximately 0.3 mM (Fourneau et al., 1924). Suramin is not metabolized by humans and persists with a rather long clearing half-life (40−50 days) (Collins et al., 1986), mainly bound to serum albumins in the blood. Suramin binding to LDL particles suppresses cholesterol and lipid uptake by the LDL receptor. The LDL receptor and glycolysis are indispensable for the parasite (Opperdoes, 1987). Consequently, considerable activity has been aimed at the cloning and overexpression of the LDL receptor and of the glycolytic enzymes (Borchert et al., 1992).

Inhibition of several trypanosomal glycolytic enzymes and weaker inhibition of the corresponding mammalian enzymes by suramin also have been demonstrated *in vitro* (Willson et al., 1993). For example, the inhibition constant for phosphoglycerate kinase (PGK) from *T. brucei* is 8 vs 150 μM for PGK isolated from other sources (Willson et al., 1993). These differences in inhibition constants presumably occur because of the striking differences in charged surface amino acids for the host and the parasite enzymes (Willson et al., 1993). Two glycolytic enzymes from *T. brucei* have been overexpressed in *Escherichia coli:* triose phosphate isomerase (TIM) (Borchert et al., 1992) and glycosomal PGK (A. E. McDermott, unpublished results). Although the *in vitro* dissociation constants for suramin on the trypanosome glycolytic enzymes are relatively weak, the hypothesis that the mode of action is glycolytic inhibition is quite reasonable if the cumulative effect of weak inhibition of all glycolytic enzymes in concert is considered. Suramin is also a weak-binding inhibitor of many enzymes whose cofactors or substrates contain phosphate groups (Stein, 1993). The toxicity of the drug is presumed to be associated with weak inhibition of kinases and topoisomerases.

Structure−activity relationships (SAR) for trypanocidal action of suramin analogs have been studied. For *T. brucei* in particular, the half molecule structures are not active, the number of rings in the structure appears to be optimized, and a variety of changes in the position or structures of ring substituents are detrimental (Nickel et al., 1986). The urea and amide linkages also are required for activity (Nickel et al., 1986). The most active compound against sleeping sickness in the SAR study was suramin itself, but numerous modifications have not yet been attempted (Fourneau et al., 1924; Nickel et al., 1986). Interestingly, these results differ from structure−activity relationships for activity against HIV (as a reverse transcriptase inhibitor) (Clanton et al., 1992; Jentsch et al., 1987; Mohan, 1993) or against cancer (binding to growth factors) (Middaugh et al., 1992; Stein, 1993). Large differences also exist between the sensitivity of *T. brucei* and other parasites to suramin analogs.

Attempts to define the structure of suramin−protein complexes by X-ray diffraction have been unsuccessful. Solution NMR studies performed by Boyle et al. clearly showed evidence of suramin binding in the basic patch and ATP binding sites of yeast PGK (Boyle et al., 1989). Aggregation of the enzymes complexed with suramin, multiple binding modes, and mixed inhibition kinetics result in poor properties of suramin−enzyme complexes for solution NMR and crystallography experiments. Fluorescence spectroscopy also has been used to study the interaction of suramin with proteins that are involved in anticancer activity of suramin (Middaugh et al., 1992).

To date the activities of suramin analogs have not been analyzed in terms of conformational preferences and conformational dynamics. For example, 10 single bonds flanking each amide linkage might be expected to be relatively rotationally unconstrained on the time scale of binding and release of the drug. In this case, binding could be enhanced for analogs that are partially or totally conformationally locked into a specific bioactive conformer. A detailed conformational analysis of suramin free in solution and bound to the protein receptors therefore is useful for rational design of analog molecules. Conformational analysis of suramin alone in solution and bound to phosphoglycerate kinases from *T. brucei* and *S. cerevisae (yeast)* is reported herein.

MATERIALS AND METHODS

Materials. Suramin was obtained as a generous gift from Professor F. Opperdoes, ICP, Université Catholique de Louvain, which in turn was a gift from Bayer. Some experiments were performed with suramin obtained from CBChemicals, Inc. (Woodbury CT), including the spectra in Figures 2−8.

Phosphoglycerate kinase from yeast (specific activity 450 units/mg) was obtained from Boehringer Mannheim and kept precipitated under ammonium sulfate.

Overexpression and Purification of Phosphoglycerate Kinase from T. brucei. Two isozymes of PGK are present in *T. brucei*: cytosolic PGK (PGKc) and glycosomal PGK (PGKg). All the experiments were done on PGKc. An efficient expression system was constructed for PGKc from *T. brucei* beginning with a *Bam*H1 and *Hind*III fragment containing the coding region. Insert for PGKc was a generous gift from the Borst laboratory. This fragment was subcloned into a mutant of the PT7-7 vector, here called PT7-71, which contained an origin of replication for single-stranded DNA (P. Michels, University of Louvain, Belgium, unpublished results). This construction contained two ATG start codons between the ribosome binding site and the coding region−one from the Nde-I site of the vector and the other from the true start signal from the *T. brucei* sequence. It was conceivable therefore to express a protein with an N-terminal extension of approximately 10 amino acids.

A mutagenesis experiment was performed to delete 35 nucleotides resulting in only one ATG, eight base pairs downstream from the ribosome binding site followed directly by the coding region. Site-directed mutagenesis was performed, using Amersham products based on the use of sulfur-

substituted nucleotides for synthesis of the first (oligo-containing) mutant strand with single-stranded DNA from the parent vector as template, followed by *Nic*I/ exonucleaseII partial digestion of the original template strand (the sulfur-containing mutant strand is immune to this digestion), and reconstruction of a second strand with the remaining fragments from the digestion as primers. The oligos consisted of an ATG flanked by the 12 base pairs of the PT7 sequence upstream and 12 base pairs of the coding sequence for PGK downstream. The oligo used for PGKc was GGAGATATACATATGACCCTTAACGAG.

Mutant colonies were screened by *Bam*H1 digestions; those which had lost the *Bam*H1 site were further screened by sequencing, yielding a mutant termed PGKc-PT7-71. Sequencing throughout the region of the mutation showed an upstream ectopic mutation that was irrelevant for the current purposes and otherwise perfect agreement.

This construction was used to transform the pLys S mutant strain of BL21 *E. coli* (Goeddel, 1990); this strain was a gift from W. Studier's laboratory. In this system expression was characterized by antibody staining, which confirmed the presence of proteins of molecular weights approximately 48 kDa for PGKc in whole cell lysates of the two transformed strains and nicely matched the results from *T. brucei* cell extracts. When partially purified by methods described below, the sensitivity of the two PGK proteins to inhibition by suramin matched the results by Misset and Opperdoes on the enzymes purified from *T. brucei* (Misset & Opperdoes, 1987).

E. coli cells were grown in 3.6 L of rich media containing 100 μg/mL ampicillin at 37 °C for 5 h, induced with IPTG at an OD_{280} of 0.3 and maintained at 37 °C for another 4 h. The cells were harvested by centrifuging at 6000*g* at 37 °C for 20 min. The pellet was resuspended in 150 mL of 50 mM MES-HCl buffer (pH 6.5) containing 1 mM EDTA, 1 mM DTT, and 100 μM PMSF. The cells were lysed by passing through a French pressure cell (9000 psi) followed by 4-fold dilution into the same buffer (total volume of 600 mL). Ammonium sulfate (40% w/v) was added, and the cell lysate was centrifuged for 20 min at 4 °C at 8000*g*. The pellet containing the cell debris and DNA was discarded. The protein was precipitated by adding 75% w/v ammonium sulfate; the pellet was resuspended into 250 mL of 50 mM Tris-HCl buffer pH 7.8 containing 1 mM EDTA, 1 mM DTT, 100 μM PMSF, and 200 mM NaCl. The remaining DNA was removed by precipitation with protamine sulfate (0.5 mg/mL final concentration), followed by centrifugation at 12000*g* for 20 min. The pellet was discarded, and the supernatant was passed through a QAE-Sephadex column (pre-equilibrated with the same buffer) twice. Fractions were collected, dialyzed against 50 mM Tris-HCl buffer, pH 7.8, containing 1 mM EDTA, 1 mM DTT, and 100 μM PMSF, and concentrated to a final volume of 30 mL. Phosphoglycerate kinase was further purified by CM-Sephadex column chromatography. The protein was eluted using a NaCl gradient (0−1 M NaCl); fractions containing the enzyme were collected and concentrated to a final volume of 10 mL. SDS/PAGE electrophoresis gel showed a single band corresponding to 45 kDa phosphoglycerate kinase, and a specific activity assay demonstrated 600 units/mg of protein. A total of 30 mg of purified PGK was obtained after the last step of purification. The protein was stored as an ammonium sulfate precipitate at 4 °C.

Sample Preparation. Suramin solutions (5 mM) were prepared in aqueous 50 mM d_{11}-Tris buffer (Cambridge Isotope Laboratories) containing 100 mM NaCl at pH 6.2. Comparable results were obtained for suramin in 250 mM phosphate buffer and 200 mM NaCl. The 0.5 mM suramin solutions were prepared in aqueous 50 mM d_{11}-Tris buffer containing 100 mM NaCl at pH 5.6.

Solutions of 5 and 0.5 mM suramin complexed with 0.5 mM and 10 μM PGK were prepared in aqueous 50 mM d_{11}-Tris buffer (Cambridge Isotope Laboratories) containing 100 mM NaCl at pH 6.2 and 5.6, respectively. Protein solutions were prepared by resuspending the ammonium sulfate precipitate in the desired buffer and dialyzing to remove the remaining ammonium sulfate. The concentration of the proteins was determined by performing activity assay and by UV spectrophotometry (at 280 nm).

NMR Spectroscopy. Two-dimensional NOESY spectra of 5 mM suramin solution were obtained on a Bruker AMX-500 operating at 500.13 MHz for protons. Water suppression was achieved using a jump-and-return read pulse (Otting et al., 1987). Two-dimensional NOESY and ROESY spectra of 0.5 mM suramin solution were obtained on a Bruker DMX-500 operating at 500.13 MHz for protons. A modified WATERGATE sequence for water suppression (Lippens et al., 1995) was incorporated into NOESY and ROESY sequences. NOESY spectra were recorded for five mixing times (50, 100, 150, 200, and 250 ms). ROESY spectra were recorded for a mixing time of 100 ms with a spin-lock field of 4 kHz. TPPI was used for frequency discrimination in the t_1 dimension (Marion & Wüthrich, 1983). Spectra were recorded as 512 × 8192 ((real) × (complex)) matrices with spectral widths of 8064 × 12 500 Hz in t_1 and t_2. Spectra were processed using FELIX (MSI). Shifted sine bells were applied in both dimensions, and polynomial baseline correction was used in the directly detected dimension. Throughout the text F1 (t_1) refers to the indirectly detected dimension while F2 (t_2) refers to the directly detected dimension. The symbol $n-m$ or σ_{nm} in reference to an NOE means that the resonance frequency corresponding to n was indirectly detected and that corresponding to m was directly detected. For buildup rates, cross peak volumes were normalized to half of the sum of the corresponding diagonal peaks, and the normalized volumes were fit to a linear function of the mixing time. In some cases, a constant offset in the peak volume was included due to artifacts (mostly t_1 ridges) in the data set.

Transferred NOESY spectra for 5 mM suramin and 0.5 mM PGK *T. brucei* were recorded for four mixing times (50, 100, 150, and 200 ms); those for 5 mM suramin and 0.5 mM yeast PGK were recorded for 50, 75, 100, and 125 ms. The jump-and-return sequence was used for water suppression. Transferred NOESY spectra for 0.5 mM suramin−10 μM PGK *T. brucei* were recorded for five mixing times (50, 75, 100, 125, and 150 ms). WATERGATE sequence (Piotto et al., 1992; Sklenár et al., 1993) and flip-back pulses (Lippens et al., 1995) were used for water suppression. TPPI was used for frequency discrimination in the t_1 dimension (Marion & Wüthrich, 1983). Spectra were recorded as 512 × 8192 ((real) × (complex)) matrices with spectral widths of 8064 × 12 500 Hz in t_1 and t_2. Spectra were processed using FELIX (MSI). Shifted sine bells were applied in both dimensions, and a polynomial baseline correction was used in the directly detected dimension.

^{13}C spin−lattice relaxation measurements were performed on natural abundance suramin at 5 mM in 50 mM d_{11}-Tris buffer in 10% D_2O at pH 6.2. Experiments were performed on a Bruker AMX-500 operating at 125.76 MHz for ^{13}C and 500.13 MHz for protons using a proton-detected double DEPT pulse sequence (Palmer et al., 1991). WALTZ-16 decoupling (Shaka et al., 1983) was applied to protons during the inversion delay. TPPI was used for frequency discrimination in the t_1 dimension (Marion & Wüthrich, 1983). Spectra were recorded as 128 × 8192 ((real) × (complex)) matrices with spectral widths of 2048 × 12 500 Hz in t_1 and t_2. Spectra were processed using FELIX (Biosym Corp., USA). Shifted sine bells were applied in both dimensions, and polynomial baseline correction was used in the directly detected dimension.

^{13}C spin−spin relaxation measurements were performed on natural abundance suramin at 5 mM in 50 mM d_{11}-Tris buffer in 10% D_2O at pH 6.2. Experiments were performed on a Bruker DMX-500 operating at 125.76 MHz for ^{13}C and 500.13 MHz for protons using a proton-detected double-DEPT pulse sequence (Palmer et al., 1991) and standard CPMG sequence during the relaxation delay (Carr, & Purcell, 1954; Farrow et al., 1994; Meiboom, & Gill, 1958). A 180° pulse was applied to protons during the CPMG pulse train (Palmer et al., 1996). The WATERGATE sequence (Piotto et al., 1992; Sklenár et al., 1993) with flip-back pulses for water suppression (Lippens et al., 1995) was incorporated into the sequence. TPPI was used for frequency discrimination in the t_1 dimension (Marion & Wüthrich, 1983). Spectra were recorded as 256 × 8192 ((real) × (complex)) matrices with spectral widths of 4096 × 12 500 Hz in t_1 and t_2. Spectra were processed using FELIX (MSI). Shifted sine bells were applied in both dimensions, and polynomial baseline correction was used in the directly detected dimension.

Light-Scattering Experiments. Light-scattering measurements were performed using a DYNAPRO-801 dynamic light-scattering instrument (Protein Solutions Inc., USA) for suramin samples in the concentration range 0.5−30 mM. The diffusion coefficient, effective molecular weight, and degree of polydispersity were calculated using built-in software, based on the assumption that the suramin molecule is spherical.

Conformational Energy Analysis. Analysis of conformational energy was performed using the MACROMODEL Interactive Molecular Modeling System (Columbia University, New York). Electrostatic charges on the suramin atoms were obtained from semiempirical and *ab initio* calculations (3-21G* basis set) using SPARTAN (Wavefunction, Irvine, CA).

Simulations of Transferred NOESY Buildup Curves. Simulations of the transferred NOESY buildup curves were performed using a program written in Mathematica (Wolfram Corp.) for each pair of protons in suramin using a 2-spin 4 × 4 relaxation-exchange matrix. The expressions for the cross peak intensities as functions of the mixing time are produced by solving the differential equation

$$\frac{dM}{dt} = -WM \tag{1}$$

where $W = R + K$ is a sum of relaxation (R) and exchange (K) matrices and M is the (4 × 1) vector describing magnetization for the two spins in the free form and the same two spins in the bound form. The general forms of these matrices can be found elsewhere (Lee & Krishna, 1992).

The solution of differential matrix eq 1 is given by

$$M(t) = \exp(-Wt)M(0) \tag{2}$$

and in the general case can be found by diagonalizing the matrix W (Campbell & Sykes 1993; Macura & Ernst, 1980)

$$M(t) = U \exp(-\Lambda\tau_m)U^{-1}M(0) = a(\tau_m)M(0) \tag{3}$$

where U is the transformation matrix that diagonalizes the W matrix; it contains eigenvectors of W as its columns; Λ is the diagonal matrix of eigenvalues; and a is a time-dependent matrix of mixing coefficients $a_{ij}(\tau_m)$, which are proportional to the integrated intensities in the transferred NOESY spectra.

Calculation of Kinetic and Relaxation Constants. The simplest case of a two-spin AX system undergoing chemical exchange between two conformations (corresponding to the free (A_f and X_f) and bound (A_b and X_b) forms of the ligand) can be represented by the following kinetic scheme:

$$A_f + X_f \underset{k_{off}}{\overset{k_{on}[E]}{\rightleftharpoons}} A_b + X_b \tag{4}$$

The relaxation matrix takes the following form (Campbell & Sykes, 1993; Landy & Rao, 1989; Lee & Krishna, 1992; Lippens et al., 1992)

$$R = \begin{pmatrix} \rho_{AA} & \sigma_{AX} & 0 & 0 \\ \sigma_{XA} & \rho_{XX} & 0 & 0 \\ 0 & 0 & (\rho_{AA})_b & (\sigma_{AX})_b \\ 0 & 0 & (\sigma_{XA})_b & (\rho_{XX})_b \end{pmatrix} \tag{5}$$

where ρ_{ii} are the spin−lattice relaxation rate constants for spin i; σ_{ij} are the cross-relaxation rate constants between spins i and j; the subscript b refers to the bound form. σ_{ij} and ρ_{ii} were calculated as a function of the effective molecular weight and proton−proton distances r_{ij} as described in the Results section. The relaxation rates for free suramin were determined from the NOESY experiments (in the case of 5 mM samples where the cross-relaxation rates are non-zero).

The exchange matrix is defined as (Campbell & Sykes, 1993; Landy & Rao, 1989; Lee & Krishna, 1992; Lippens et al., 1992):

$$K = \begin{pmatrix} k_1 & 0 & -k_2 & 0 \\ 0 & k_1 & 0 & -k_2 \\ -k_1 & 0 & k_2 & 0 \\ 0 & -k_1 & 0 & k_2 \end{pmatrix} \tag{6}$$

k_1 is a pseudo-first-order rate constant determined by k_{on} and [E], the concentration of free enzyme: $k_1 = k_{on}[E]$. [E] in turn is calculated $[E] \approx [E]_T K_d/([L]_T + K_d)$, where $[E]_T$ is the total concentration of the enzyme, $[L]_T$ is the total concentration of the ligand or the substrate, and K_d is the dissociation constant. Equivalently, k_1 can be defined using k_{off} and $f = [EL]/[L]_T$, the fraction of the bound ligand: $k_1 = k_{off} f$. k_2 is the release constant, also called k_{off}, which can also be expressed as $k_2 = k_{on}K_d$. $[E] \approx ([E]_T/[L]_T)K_d$ if $[E]_T \ll [L]_T$; thus $k_1 \approx k_2[E]_T/[L]_T$ for a simple binding mechanism involving weak dissociation constants.

Thus, the free parameters in the simulation, σ_{ij}, ρ_{ii}, k_1, and k_2 can be calculated from the more fundamental and experimentally accessible parameters, r_{ij}, k_{on}, $[E]_T$, $[L]_T$, K_d,

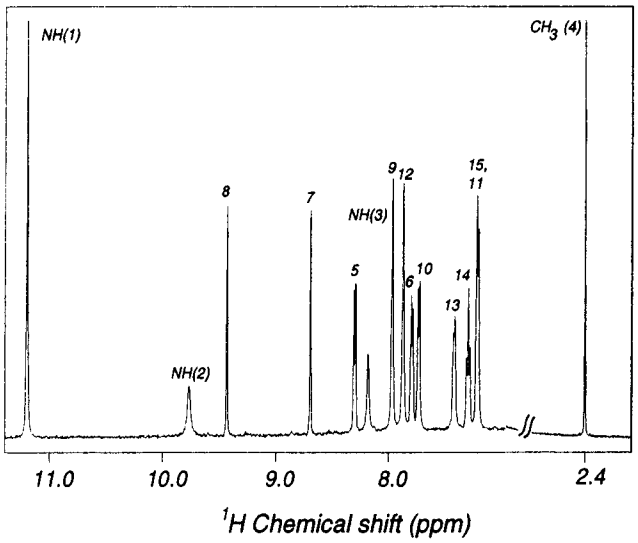

FIGURE 2: 1D proton NMR spectrum of suramin at 5 mM (the sample was prepared in 50 mM d_{11}-Tris buffer containing 100 mM NaCl at pH 6.2).

and the molecular weights. The rate constants were obtained using close to the diffusion-limited bimolecular binding rate k_{on} of 10^8 M^{-1} s^{-1}, reported for several enzyme−ligand binding kinetics measurements (Hammes & Schimmel, 1970), and suramin−PGK binding constants reported in the literature (Willson et al., 1993). The relaxation rates, ρ_{ii} and σ_{ij}, for bound ligand were calculated using data for intra-aromatic calibration distances, assuming correlation times to be those of the protein and absence of internal motions in the bound state. As discussed below, the resulting "over-constrained" simulations have miserable agreement with the data. Satisfactory agreement with data was achieved only if the ratio of kinetic constants k_1 and k_2 was allowed to differ substantially from these calculations. That this ratio differs from the calculated ratio is surprising and is discussed further in the Results section. Furthermore, the overall scaling of these constants had to be varied freely, which corresponds to allowing k_{on} to vary freely. Variation in $[E]_T$, $[L]_T$, and K_d ALONE (while utilizing simple equilibrium calculations as outlined above) could *NOT* produce satisfactory simulations. Kinetic parameters reported here are those that produced the best fit to the experimental buildup curves for the calibration (intra-aromatic) cross peaks. For other protons, these kinetic parameters were kept invariant, in order to determine the relaxation rates for bound suramin and thereby generate distance constraints.

The Mathematica notebooks for simulations of the transferred NOESY buildup curves can be found on the following Web site: http://www.chem.columbia.edu/~mcdhome/abstracts/NOE.html.

RESULTS AND DISCUSSION

Free Suramin: *Chemical Shift and Assignments*. The structure of suramin is shown in Figure 1. The 1D solution proton NMR spectrum of suramin at 5 mM is shown in Figure 2 (with proton numbering corresponding to that in Figure 1). For 5 mM suramin one peak per chemically equivalent proton (i.e. per proton in the half-molecule) is observed. This implies that the molecule either has a unique and symmetric conformation or (more likely) is in rapid equilibrium between a family of conformations resulting in average chemical shifts. The three amide protons with chemical shifts of 11.3, 9.8, and 8.2 ppm were detectable below pH 7. The resonance of the amide proton 1 (11.3 ppm) is extremely deshielded due to a strong hydrogen bonding to a neighboring sulfonate group. In addition, this resonance is observable even at mildly basic pH values, indicating that proton exchange rates with the solvent are unusually low, and therefore the hydrogen bond is quite strong. The two upfield amides are only detected below pH 7, and the intensities increase with increasing acidity. The rate of exchange of the amide protons at pH 6.2 is on the millisecond time scale, and the two upfield amide proton resonances are partially saturated if water suppression is achieved via a long saturating pulse during the relaxation delay. Therefore, solvent suppression was performed utilizing "jump-and-return" methods (Otting et al., 1987) or modified WATERGATE sequences with flip back pulses (Lippens et al., 1995) and pulsed field gradients.

For suramin at a concentration of 0.5 mM, the chemical shifts are different from those for the 5 mM sample. In this case (as for the 5 mM samples) only one peak per chemically equivalent proton is observed. For the more dilute samples, spectra were taken under mildly acidic conditions (pH 5.6) so that all three amides could be detected. A high salt concentration (100 mM NaCl) was used to keep the ionic strength close to physiological conditions and also in order to improve the resolution of the aromatic peaks. However, the pairs of peaks 9 and 12, as well as 14 and 15, were still partially overlapped.

J couplings measured from a DQ-filtered COSY were used to identify the aromatic peaks because the coupling patterns are different for each ring. The assignments were confirmed and ambiguities resolved using NOESY spectra.

At 10 °C, resonances of 5−20 mM suramin were broadened dramatically; this presumably reflects further aggregation of suramin to form large micelles, as discussed below.

Aggregation of Suramin. Typical 2D NOESY spectra for suramin at 5 and 0.5 mM concentration are shown in parts a and b of Figures 3, respectively. Buildup curves were measured for every pair of protons of suramin at 5 mM, and normalized cross peak volumes as a function of mixing time for amide-to-aromatic proton pairs are shown in Figure 4. The NOE buildup rates, given in Table 1, are the linear slopes estimated from least-squares fitting. In suramin there are several pairs of protons within one aromatic ring which have a known distance (2.46 Å), and these were used to calibrate the NOE measurements and estimate the rotational correlation time (which was assumed to be isotropic), using the following expression (Palmer et al., 1993)

$$\sigma_{n-m} = \frac{1}{4}\left(\frac{\mu_0}{4\pi}\right)^2 \hbar^2 \gamma_H{}^4 r_{nm}{}^{-6}[6J(2\omega_H) - J(0)] \qquad (7)$$

$$J(\omega) = \frac{2}{5}\left[\frac{S^2\tau_m}{1+(\omega\tau_m)^2} + \frac{(1-S^2)\tau}{1+(\omega\tau)^2}\right]$$

$$\tau = \left[\frac{1}{\tau_m} + \frac{1}{\tau_e}\right]$$

in which γ_H is the proton gyromagnetic ratio, $\hbar$ is the reduced Planck's constant, r_{nm} is the distance between the *n*th and

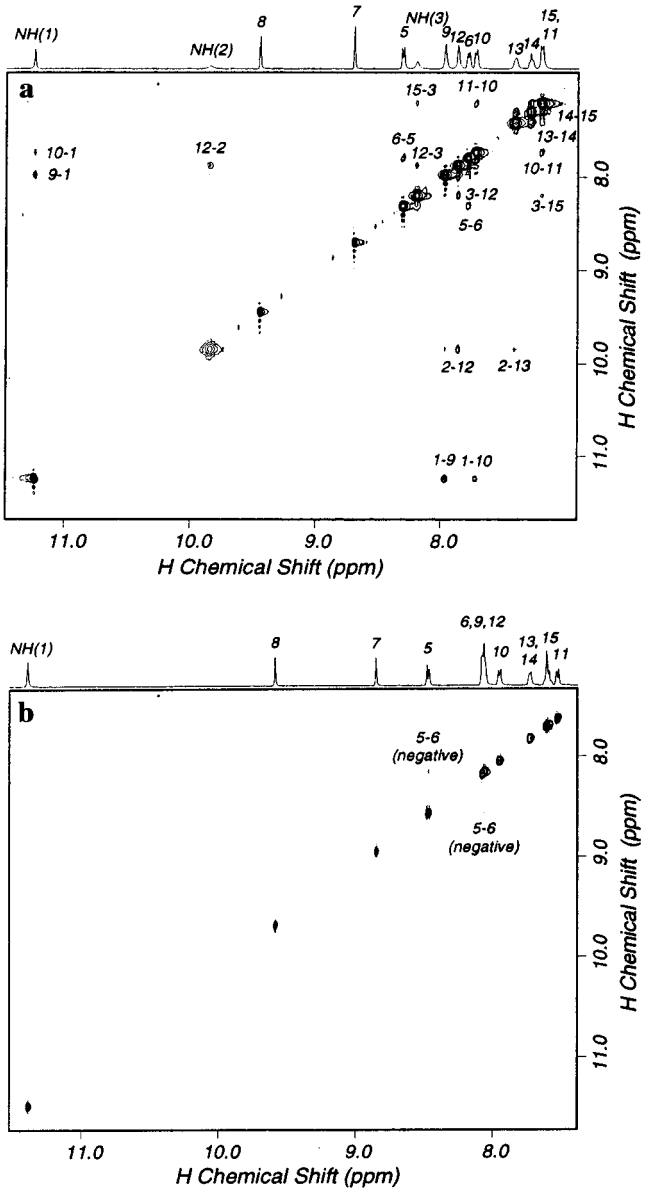

FIGURE 3: NOESY spectrum of suramin in 50 mM aqueous d_{11}-Tris buffer containing 100 mM NaCl: (a) At 5 mM and pH 6.0. The water peak was suppressed with a jump-and-return sequence. The mixing time was 100 ms. (b) At 0.5 mM and pH 5.6. The water peak was suppressed using modified WATERGATE sequence. The mixing time was 100 ms. No cross peaks for 0.5 mM suramin are observable that involve amides. The calibration cross peaks (e.g. 5−6 and 6−5) are very small and negative (e.g. positive NOE or faster tumbling than the cancellation condition).

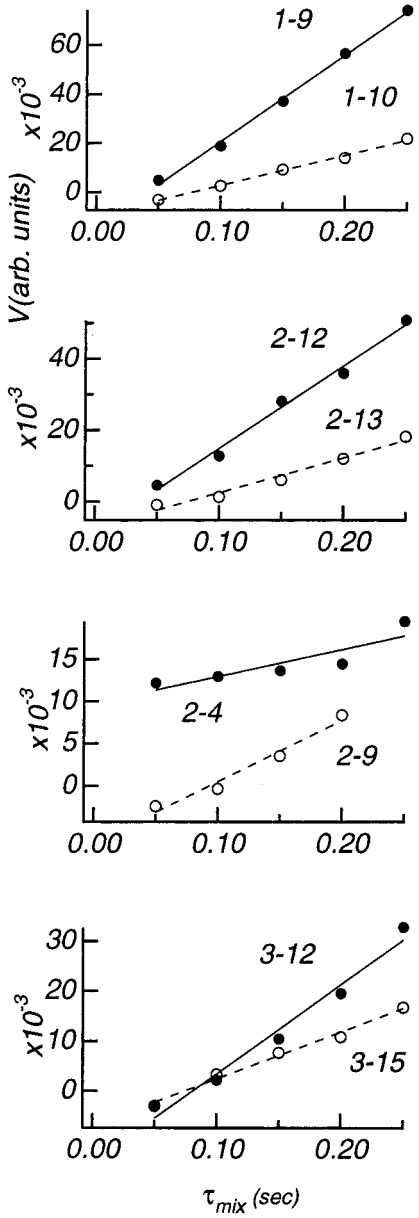

FIGURE 4: NOE buildup curves for 5 mM suramin, indicating the normalized cross peak volume vs mixing time for the amide-to-aromatic proton pairs showing the contributions from different conformers to the NOE.

the *m*th protons, μ_0 is the magnetic permeability of vacuum, $J(\omega)$ are the spectral density functions, τ_m is the overall rotational correlation time of the molecule, τ_e is the effective internal correlation time, and S^2 is the generalized order parameter (Lipari & Szabo, 1980; Lipari & Szabo, 1982; Lipari & Szabo, 1982).

Buildup rates for various pairs of protons of interest as well as the apparent correlation times for the proton pairs that have a fixed distance are presented in Table 1 (calculated assuming S^2 to be 1). Unexpectedly, the apparent correlation times (indicated with a single asterisk in Table 1) vary widely throughout the molecule. This variation could result from an artifact in the peak normalization for overlapping peaks (11 and 15), from multispin dynamics, from internal degrees of conformational freedom, or from anisotropic tumbling.

Carbon spin−lattice relaxation measurements were used to establish whether various rings of the molecule are actually characterized by different correlation times. The results of ^{13}C T_1 measurements are presented in Table 2. The relaxation curves for carbons 7 and 13 are given in Figure 5. These carbon relaxation rates were interpreted including dipolar and CSA relaxation (Palmer et al., 1993)

$$\frac{1}{T_1} = \frac{1}{4}\left(\frac{\mu_0}{4\pi}\right)^2\left(\frac{\hbar^2\gamma_H{}^2\gamma_C{}^2}{10}\right)r^{-6}[J_0(\omega_H - \omega_C) + 3J_1(\omega_C) + 6J_2(\omega_H + \omega_C)] + \frac{(\omega_C(\sigma_{||} - \sigma_\perp))^2}{3}J_1(\omega_C) \quad (8)$$

where γ_C is the carbon gyromagnetic ratio, $r = 1.1$ Å is the C−H bond length, $\omega_C = 125.76$ MHz, $\sigma_{||} - \sigma_\perp = -172$ ppm ($\sigma_{||}$ and $\sigma_\perp$ are the parallel and perpendicular components of the chemical shift tensor). The relaxation times and the

Table 1: NOE Buildup Rates for Suramin[a]

proton t_2	proton t_1	σ_{12} (±20%) (s^{-1})	$R_{assumed}$, Å	τ_c, ns[b]	R_{pseudo}, Å (±0.5 Å) (τ_c based on ^{13}C relaxation)[c]	R_{pseudo}, Å (±0.5 Å) (τ_c from closest calibration peak)[d]
1	9	−0.353			2.75	2.30
1	10	−0.123			3.28	2.74
2	4	−0.032			4.10	3.25
2	9	−0.073			3.58	2.83
2	12	−0.232			2.95	2.34
2	13	−0.098			3.41	2.70
3	12	−0.178			3.08	2.91
3	15	−0.094			3.43	3.24
4	2	−0.025			4.28	3.39
5	6	−0.245	2.46	1.10	2.92	2.45
6	5	−0.218	2.46	1.01	2.98	2.49
9	1	−0.579			2.53	2.12
9	2	−0.097			3.41	2.70
10	1	−0.208			3.00	2.51
10	11	−0.182	2.46	0.82	3.07	2.43
11	10	−0.155	2.46	0.79	3.16	2.50
12	2	−0.279			2.86	2.27
12	3	−0.209			3.00	2.84
13	2	−0.133			3.24	2.56
13	14	−0.493	2.46	2.02	2.60	2.45
14	13	−0.431	2.46	1.78	2.66	2.52
14	15	−0.499	2.46	2.04	2.60	2.46
15	3	−0.111			3.34	3.15
15	14	−0.522	2.46	2.13	2.58	2.48

[a] For the calibration peaks (5−6, 6−5, 10−11, 11−10, 13−14, 14−13, 14−15, 15−14) the buildup rates were used to compute effective correlation times. For other peaks, the correlation times of 2.74 ns (obtained from the carbon relaxation measurements), and those obtained from the closest calibration NOE, were used to compute effective distances. Equations 7 and 8 were used with the assumption of an internally rigid structure (order parameter (S^2) of 1.0). Note that the correlation times obtained from the NOE are generally lower than those obtained from the carbon relaxation rates. [b] These correlation times of the calibration peaks were calculated assuming $S^2 = 1$ and a fixed distance of 2.46 Å for aromatic-to-aromatic protons. [c] These distances were calculated assuming 2.74 ns correlation time (mean correlation time obtained from ^{13}C relaxation experiments). [d] These distances were calculated using the closest proton calibration pair: the average of 13-14 14-13 14-15 and 15-14 was used for distances involving amide 3; the average of 10-11 and 11-10 was used for distances involving amide 2; the average of 5-6 and 6-5 was used for distances involving amide 1.

Table 2: Carbon Relaxation Times for 5 mM Suramin[a] and Rotational Correlation Times Derived Using Eq 8, with the Assumption of an Internally Rigid Structure (Order Parameter (S^2) of 1.0)

carbon no.	T_1, s (±20%)	τ_{cor}, ns[b]	$I^\infty/I(0)$
5	0.214	2.63	0.2605
6	0.207	2.49	0.2653
7	0.233	2.97	0.2521
8	0.217	2.69	0.2588
9	0.238	3.06	0.3014
10	0.207	2.50	0.2660
11	0.239	3.07	0.3196
12	0.231	2.93	0.2969
13	0.202	2.40	0.2876
14	0.223	2.80	0.2872
15	0.214	2.64	0.2794

[a] Measured from the HSQC experiment—see Figure 5. [b] The correlation times were calculated from eq 2 assuming dipolar and chemical shift anisotropy relaxation mechanisms (with uniaxial CSA and isotropic motion) and $S^2 = 1$ as explained in the text.

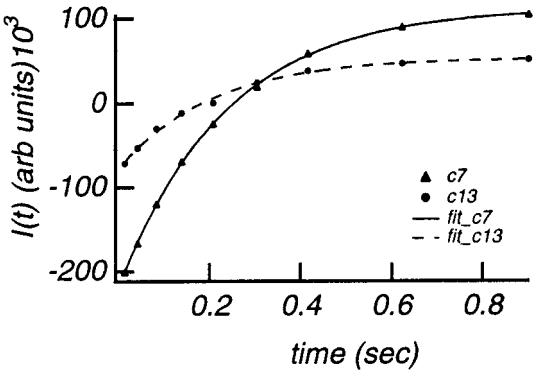

FIGURE 5: Experimental points and fitted curves for ^{13}C spin−lattice relaxation of carbons 13 (●) and 7 (▲) of suramin. Data were fit to the expression $I(t) = I^\infty - [I^\infty - I(0)] \exp(-t/T_1)$ where I^∞ is the steady-state intensity (at "infinite" time), $I(0)$ is the initial intensity, and T_1 is the carbon spin−lattice relaxation time. The ratio $I^\infty/I(0)$ and the value for T_1 are given in Table 2. The estimated error (20%) corresponds to the relaxation rates for which the fit error (measured as χ^2) is double that for the best fit. As such, they are rather generous estimates.

derived correlation times (calculated assuming $S^2 = 1$) are given in Table 2.

Internal motions or asymmetric tumbling may play a role in the variability of the NOE calibration values but do not cause as dramatic a variation on the carbon relaxation times (discussed in the next section).

The rotational correlation times given by the carbon relaxation measurements are in the range 2.4−3.1 ns (when S^2 is assumed to be 1), a much narrower range than that indicated by the NOE data. The average values suggest a molecular weight of approximately 6000, which is much larger than the monomeric weight of 1429 (in agreement with the NOE values). Therefore, we concluded that suramin is multimeric at 5 mM and at room temperature; the dominant form appears to be tetrameric. Additional confirmation of the aggregation was obtained by measuring the field dependence of the NOEs; when 200, 300, and 400 MHz spectrometers were utilized, no cancellation condition for the NOEs could be found. For suramin at 0.5 mM the NOESY spectrum shows no or very small negative NOE cross peaks. This is indicative of a molecular weight near the NOE cancellation condition and suggests a monomeric state of

suramin at this concentration. Light-scattering measurements show the effective molecular weight of suramin to be in the range 2−4 kDa for suramin concentrations 5−30 mM, also indicating a multimeric state. No scattering signal was observable for 0.5 mM suramin, also consistent with the hypothesis that suramin is not aggregating appreciably at this concentration.

Conformational Analysis: (1) Molecular Mechanics Simulations. For each of the molecular fragments in Figure 8, the energies of the structures as a function of the corresponding dihedral angles were calculated using MACROMODEL and the results analyzed in a form of Ramachandran plots. The atomic charges were derived from semiempirical and *ab initio* calculations in SPARTAN and used for simulating the conformational energies in MACROMODEL. Although the resulting charges from semiempirical calculations differed from the *ab initio* charges for the sulfonate groups and amide fragments of the molecule, the differences did not have significant impact on the results of the simulations. For each of the fragments analyzed several broad conformational minima exist, so significant conformational freedom is expected for each conformer. Planar structures do not appear to be at the energy minima, as expected based on steric considerations. (Crystallographic studies have also shown that the aromatic rings do not ordinarily lie in the plane of the amido group in analogous compounds (Brisson & Brissé, 1985; Ganis et al., 1971; Kashino et al., 1979).) Aromatic-to-amide distances vary from 1.75 to 4.6 Å as a function of the corresponding dihedral angle. However, distances in the range 1.75−2.0 Å are associated with steric conflicts, and thus the near-planar structures can be neglected. For example, to resolve steric clashes between proton pairs 1−9 and 1−10 the molecule might adopt a 20−30° out-of-plane conformation (see dihedral angle χ_1 in Figure 1: 30° represents the energetic minimum in a Ramachandran plot from MACROMODEL; the conformational minimum extends from 23 to 50° out-of-plane). For dihedral angle χ_2 the calculations predict highly nonplanar structures (with the minima typically around 76° out-of-plane). For the degrees of freedom characterized by both χ_3 and χ_4, the conformational minima are between 0 and 50° according to MACROMODEL. The differences in energy between the maxima and the minima are of the order of 5−7 kcal/mol for χ_1, χ_3, and χ_4 and 18−20 kcal/mol for χ_2, but the minimum energy reaction coordinates connecting the minima generally have barriers of the order of 2−5 kcal/mol. Despite the fact that the positions of the conformational minima from the simulations are in good agreement with the NOE data (discussed in detail in the following sections), the populations were not reproduced. For example, two possible conformers exist for the degree of freedom characterized by χ_1: conformers I and II in Table 3. According to the experimental data (discussed in the following sections), there is a pronounced preference toward conformer I in the free suramin. Macromodel calculations, however, do not account for the observed preferences and generally indicate equal populations for the two conformers.

(2) NOE Calibration. The pseudodistances given in Table 1 were determined using the NOE buildup rates and the rotational correlation times determined either from the carbon relaxation measurements or the calibration NOE strengths and were interpreted in terms of eq 7 (where the order parameter is assumed for the moment to be 1). These pseudodistances are not likely to be actual distances in most cases. The calibration peaks for the proton NOE values vary dramatically in their buildup rates or inferred correlation times. When the correlation time measured from carbon relaxation experiments (2.74 ns) is used in eq 7, the predicted distances for the calibration pairs of protons (5−6, 10−11, 13−14, 14−15) do not fall into the expected range 2.45−2.55 Å, but range from 2.58 to 2.66 Å for the calibration peaks 13−14, 14−15, and are as long as 3.1 Å for the calibration peaks 5−6 and 10−11. This systematic error presumably reflects internal conformational dynamics and gives rise to an error in the NOE−derived distances of at least 0.5 Å.

Table 3: Two Limiting Conformations for Three of the Single-Bond Dihedrals[a]

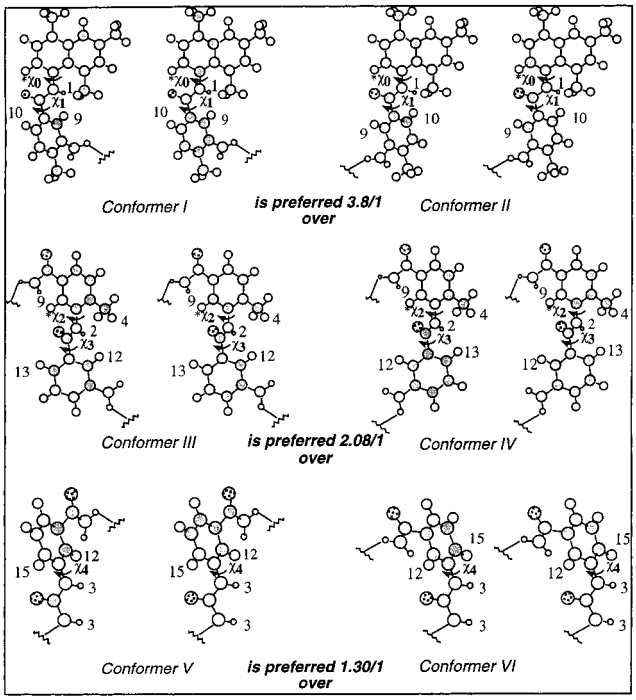

[a] The relative populations of the conformers are indicated, as determined from the amide-to-aromatic NOE buildup curves. To determine these ratios, a variety of assumptions about the degree of nonplanarity and the disorder of the molecule must be made.

Multispin dynamics does not account for the variations in the proton cross-relaxation rates of the calibration cross peaks as was confirmed by spin dynamics calculations involving 2−7 spins in appropriate geometries (Polenova, 1997). In order to understand whether these variations arise from internal conformational dynamics, we analyzed the trends in the ^{13}C spin−lattice and spin−spin relaxation rates for suramin carbons measured experimentally to compare them to the proton cross-relaxation rates from NOEs. The ^{13}C spin-spin relaxation rates are given in Table 5. We have analyzed the relaxation rates (NOEs and spin−lattice and spin−spin relaxation rates) predicted using Lipari−Szabo formalism as functions of S^2 (generalized order parameter) and τ_e (internal correlation time) for τ_m (rotational correlation time) of 2.74 ns as derived from ^{13}C T_1 measurements. Proton−proton NOEs and ^{13}C T_2s behave as monotonous functions of S^2 and τ_e; the rates increase with increasing either S^2 or τ_e where τ_e is assumed to be in the range of picoseconds to nanoseconds. Spin−lattice relaxation rates are faster for larger S^2's in the range of τ_e from picoseconds to about 2

ns; the derivative of the function changes sign for the internal correlation times slower than 2 ns. On the basis of this information, trends for the NOE cross-relaxation rates of the calibration protons should be similar to those for the spin−lattice relaxation rates and depending on the time scales of the internal dynamics be either similar or opposite to the trends in the spin−spin relaxation rates. According to the experimental data (Tables 2 and 5), there are no correlations between proton−proton cross-relaxation and carbon spin−lattice and spin−spin relaxation rates. However, this does not rule out the possibility that internal dynamics are responsible for the variations in the cross-relaxation rates of the calibration protons. Slow motions are probably present and would not be well accommodated in this model. Also, the geometry of the problem must be considered in more detail than the Lipari−Szabo formalism allows; i.e. the bonds and rotational axes have arbitrary relative orientations. Even more sophisticated treatment will be required if the molecule forms aggregates with a distribution of molecular weights (Schurr et al., 1994).

Nonetheless, we attempted to describe the internal dynamics in suramin within the Lipari−Szabo formalism, using ^{13}C R_1, ^{13}C R_2, and ^{1}H NOE data. Molecular mechanics calculations (described above) indicate that the amide fragments are free to rotate within broad conformational minima. Therefore, our initial assumption of the order parameter $S^2 = 1$ (Lipari & Szabo, 1980; Lipari & Szabo, 1982; Lipari & Szabo, 1982; Palmer et al., 1993) (see eqs 7 and 8) is not justified. The experimental data as well as molecular mechanics calculations suggest using the diffusion in a cone model, angular excursions of the bond vectors of 30° or greater (Lipari & Szabo, 1980; Lipari & Szabo, 1982; Lipari & Szabo, 1982; Palmer et al., 1993) resulting in S^2 below 0.65. On the basis of the known distances for calibration peaks (5−6, 10−11, 13-14, 14−15) and those for the C−H bond lengths, and assuming the overall tumbling to be isotropic, we interpreted the relaxation and NOE data (eqs 7 and 8) to yield a value of S^2 and an internal correlation time for each carbon (5, 6, 10, 11, 13, 14, 15). Using these lower values of S^2 results in agreement between the correlation time extracted from carbon T_1 data and the NOE data if suramin is assumed to be pentameric (using a rotational correlation time of 2.8 ns); this agreement was not possible with the assumption of internal rigidity. In this model the S^2 values for the middle two aromatic rings are in the range 0.55−0.6 and for the outer two rings in the range 0.12−0.27. The internal correlation times were all of the order 0.3−0.5 ns. The Lipari−Szabo formalism may be inaccurate since the correlation times approach the overall rotational correlation time, and $\omega_H\tau_c \sim 1$; in addition the order parameters are very low. There was no consistent solution for all three data sets, that is R_1, R_2, and NOE data.

There have been several approaches for analyzing the contributions of motions on different time scales to the relaxation rates beyond Lipari−Szabo treatment; those include mapping of spectral densities (Peng & Wagner, 1992a; Peng & Wagner, 1992b) and quasi spectral density function analysis (Ishima & Nagayama, 1995). These methods are based upon reducing the number of independent variables (spectral densities) in the expressions for the relaxation rates and thus making the set of experimentally measured rates sufficient to extract the time scales of the motions of the system. In the case of suramin the approach will not provide additional insight on the problem because we are dealing with ^{13}C, rather than ^{15}N, relaxation rates (and the approximations are too crude). In the case of proton cross-relaxation rates we have an additional term $J(2\omega_H)$ which cannot be approximated. Therefore, the number of the variables in the system will not be reduced, and the problem is grossly underdetermined.

For the purposes of the following discussion we have set the correlation time to a mean value of that found for the closest calibration peak as explained in the last column of Table 1 (e.g. for correlations involving amide 3 we used the NOE involving protons 13−15 to calibrate the distance, for correlations involving amide 2 we used the calibrations involving protons 10 and 11, and for correlations involving amide 1 we used the calibrations involving protons 5 and 6). This is tantamount to assuming that the internal dynamics are the major source of variation and that the dynamical properties of a given amide can be approximated by the dynamical properties of the closest ring; clearly this assumption will give rise to approximate results but in all probability is better than using the correlation time derived from the carbon relaxation rates which gave rise to errors of ±0.5 Å. In fact, this choice does not have a dramatic impact upon the final conclusions about preferred conformers.

(3) Conformational Analysis for Specific Degrees of Freedom. The drug evidently is rapidly interconverting between several conformers, and therefore the NOEs must be considered as averages of weighted sums from all of these species. The evidence for the presence of multiple conformers in dynamic equilibrium is as follows. Every proton is associated with only one chemical shift, indicating either fast averaging between several structures or a single symmetric structure. However, the observation of strong NOEs connecting a particular amide to two protons from a neighboring aromatic group cannot be rationalized by assuming a single symmetric conformation of suramin. For example, amide 1 has pseudodistances of 2.30 and 2.74 Å to protons 9 and 10, on opposite sides of the ring, which is not simultaneously possible. Interpretation of the results in terms of rapidly exchanging conformers is the simplest approach to analyze the data in a consistent fashion. Relatively low barriers are expected for the single bonds, as discussed above, so this interconversion is not particularly surprising.

For several local degrees of freedom (χ_1, χ_3, χ_4), two limiting conformers are presented in Table 3, and both contribute to the NOE cross-peak intensities. Their characteristics (including dihedral angles, populations, and flexibility) are described below. Since the chemical exchange is in the rapid limit, the phenomenological cross-relaxation rate constants are given by population-weighted average rate constants for individual conformers (eq 6) (Ni, 1994)

$$\sigma_{ij} = p^{I}\sigma^{I}_{ij} + p^{II}\sigma^{II}_{ij} \qquad (9)$$

$$\sigma_{ik} = p^{I}\sigma^{I}_{ik} + p^{II}\sigma^{II}_{ik}$$

where σ_{ij} and σ_{ik} are the experimental exchange rate constants for cross-relaxation between the amide proton i and the aromatic protons j and k; σ^{I}_{ij}, σ^{II}_{ij}, σ^{I}_{ik}, σ^{II}_{ik} are expected theoretical rate constants for the two conformers, and p^I and p^{II} are the corresponding populations ($p^I + p^{II} = 1$). An extrapolation of this expression to many conformers can be constructed.

We have made the assumption that the average degree to which the dihedral is out of plane is the same for the two conformers corresponding to each degree of freedom. In general the NOE to the more distant proton can be ignored for each conformer (for example in Table 3, conformer I, the 1−10 NOE can be neglected). With these two assumptions the extent to which each aromatic ring is out of plane with respect to the adjacent amide can be estimated by adding the two NOEs, e.g. the sum of the buildup rates for the proton pairs 9−1 and 10−1 (normalized to the closest calibration peak) can be used to estimate the extent to which that degree of freedom is out of plane. In this analysis dihedral χ_1 is approximately 35° out of plane since the average amide−aromatic distance is 2.01 Å, χ_2 is between 80°and 40° out of plane and probably differs for the two conformers in this case since the average amide−aromatic distance is 2.60 Å, χ_3 is approximately 40° out of plane since the average amide−aromatic distance is 2.12 Å, and χ_4 is approximately 50° out of plane since the average amide−aromatic distance is 2.64 Å.

Conformational preferences for the individual degrees of freedom ($\chi_0 - \chi_4$, Figure 1) are discussed separately below in terms of the NMR data. The degrees of freedom of suramin are roughly independent of one another according to modeling calculations, and furthermore the NMR data only permit a study of local correlations. However, isolating each dihedral angle is an oversimplification, and some specific combinations result in steric or electrostatic conflicts. We find clear evidence for multiple conformations in several of these degrees of freedom (χ_1, χ_2, χ_4), and thus the combinatorial concatenation of all of these possibilities leads to a vast number of molecular conformations. These conformers differ significantly from each other in overall shape and charge patterns; we presume that most of them are present in aqueous solution, both at 5 and at 0.5 mM, although we cannot accurately predict their relative concentrations.

(A) Dihedral Angle χ_0. The dihedral angle χ_0 relates the naphthalenesulfonic acid to the outermost amide. NOE buildup rates support the hypothesis that the outermost amide N-to-aromatic single bond is rotationally fixed as indicated in Figure 1; this is based upon the observation that no NOEs are observed between amide 1 and aromatic protons on the naphthalene. In addition, proton 1 is very deshielded and has a very slow exchange rate with bulk solvent (less than ca. 1 s^{-1}) as would be expected for a strongly hydrogen bonded structure.

(B) Dihedral Angle χ_1. The degree of freedom around χ_1 is described in terms of two limiting conformations in Table 3, one in which the amide proton 1 is facing the aromatic proton 9 (I) and one in which the amide proton 1 is facing aromatic proton 10 (II). The NMR data indicate a clear preponderance of structure I over II, both for the 5 mM data and the 0.5 mM data.

In order to estimate the equilibrium mixture of two conformers I and II (Table 3), we had to make the assumption that the extent to which the molecule is out of plane is similar for I and II. If both are about 35° out of plane (as indicated by the modeling calculations), the closest N−H Ar−H distances would be about 2.0 Å and the expected rates $\sigma^{I}_{1-9} \approx \sigma^{II}_{1-10} \approx 0.79$; and $\sigma^{II}_{1-9} \approx \sigma^{I}_{1-10}$ are quite small and can be neglected within our experimental error. Since σ_{9-1} is 0.57 and σ_{10-1} is 0.21, we conclude that the populations p^{I} and p^{II} are approximately 73% and 27%, respectively. However, the errors in this estimate are significant. Significant systematic experimental errors are associated with extracting cross-relaxation rates from the NOE volumes (due to additional cross-relaxation pathways) and are hard to estimate; these errors impact the population estimates linearly. Furthermore, the assumption that both conformers are out of plane to the same extent is a simplification. Only crude boundaries on these angles may be deduced. The 9−1 and 10−1 NOEs are fairly large (that is they sum to 0.79); therefore the conformers with approximately 35° dihedral angles are preferred and those conformers with larger dihedral angles and smaller NOEs are poorly populated. Molecular modeling would also suggest that conformers with dihedrals less than about 10° or more than 50° are also poorly populated since the estimated energies are more than *kT* above the global minimum.

The energetic preference for I over II cannot be satisfactorily explained based on either simple geometrical considerations or molecular mechanics calculations of the energy as a function of dihedral angles χ_1, χ_0, and χ_2, computed using MACROMODEL with AMBER force field (see above). The answer to the question why I is preferred over II is unclear but would seem to have an electrostatic basis and thus might be strongly influenced by the protein environment to which the drug binds.

(C) Dihedral Angle χ_2. The energetics for χ_2 (see Figure 1) differ from those for χ_1 in that an additional methyl group in the ortho position to the amide fragment is responsible for stronger steric conflicts with either the amide proton 2 or the nearby carbonyl oxygen. The clash can be avoided if dihedral χ_2 adopts a value of about 50° within the broad minimum from 20 to 90°. Our experimental data suggest even further deviations from planarity: we observed very weak NOEs for 9−2 and 4−2 which sum to approximately 0.12 s^{-1}. The corresponding distance is above 3 Å, or an angle is between 60 and 90° out of plane. Of course, the range of structures compatible with this nonplanarity is significant, and there is no apparent energetic preference for the two distinct perpendicular structures based on the modeling calculations.

(D) Dihedral Angle χ_3. Dihedral angle χ_3 is illustrated in Figure 1 and in Table 3 with the structures III and IV. P^{III} σ^{III}_{12-2} and P^{IV} σ^{IV}_{13-2} sum to approximately 0.41, thus suggesting an average amide−aromatic distance of 2.12 Å and the dihedral would be ca. 40° out of plane and that the populations P^{III} and P^{IV} are 68% and 32%, respectively; considerable error is expected, for the same reasons as discussed above in connection with χ_1. The overall weaker NOE might suggest a larger dihedral angle than for χ_1, but might also be associated with a faster exchange rate for amide proton 2 or experimental error. MACROMODEL calculations suggest χ_3 would prefer values of approximately 30° out-of-plane, with a particularly broad minimum (+60 to −60° are within *kT* of the global minimum), and no preference of III over IV.

(E) Dihedral Angle χ_4. Dihedral angle χ_4 is shown in Figure 1, and the limiting structures V and VI are shown in Table 3. Nonplanarity is again implied by the NOE data: (σ^{VI}_{12-3} and σ^{V}_{15-3}) sum to 0.32s^{-1} corresponds to 2.64 Å distance and 50° out of plane on average. The estimated populations are $P^{VI} = 65\%$ and $P^{V} = 35\%$ which are within experimental uncertainties of being equal. For this fragment molecular mechanics calculations indicate a very broad minimum near 30° out of plane, with no preference for V

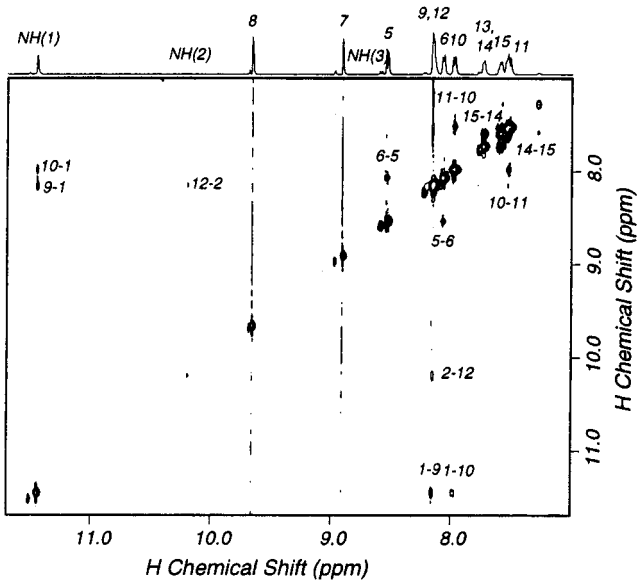

FIGURE 6: ROESY spectrum of suramin at 0.5 mM in 50 mM d_{11}-Tris buffer containing 100 mM NaCl at pH 5.6. Mixing time is 100 ms. B_1 field strength is 4 kHz. Cross peaks are of opposite sign relative to the diagonal peaks.

or VI. When structure VI is adopted on both sides of the molecule, the overall conformation is quite compact and buries significant hydrophobic area. Experimental data do not indicate that these structures are significantly different in energy from others.

Suramin Conformation at 0.5 mM. NOE buildup curves could not be obtained for suramin at 0.5 mM because at this concentration the NOE cancellation condition is reached. However, some of the important cross peaks could be seen in the ROESY spectrum of 0.5 mM suramin (Figure 6). For these ROESY cross peaks, the agreement with the NOESY data at 5 mM was quite good. In Figure 7, 1D slices from various spectra are displayed: the NOESY spectra of 5 and 0.5 mM suramin and the ROESY spectrum of 0.5 mM suramin (a, b, and c, respectively) are given to illustrate the similarities in ratios of intensities of the cross peaks 1−9 and 1−10. Thus, the preferred conformational distribution of suramin is probably invariant with concentration and aggregation state.

Suramin Complexed with the Enzymes. Proton Spectra of Suramin in the Presence of Phosphoglycerate Kinases. The proton chemical shift values observed for both 5 and 0.5 mM suramin are essentially invariant in the presence of phosphoglycerate kinase; the amide peaks are broadened in the presence of the enzymes, implying faster exchange rates with the solvent (data not shown). There is still one peak per chemically equivalent proton observed in the spectrum in the presence of PGK, just as for the free compound.

Transferred NOESY Spectra of Suramin−PGK Complexes. Transferred NOESY spectra for a sample containing a mixture of 5 mM suramin−0.5 mM PGK *T. brucei*; a sample containing 0.5 mM suramin−10 μM PGK *T. brucei*; and 5 mM suramin−0.5 mM yeast PGK for the mixing time of 100 ms are shown in Figure 9 (a, b, and c, respectively). There are no new features in the transferred NOESY spectra of suramin complexes compared to the NOESY spectra of the free suramin; cross peaks in the spectra of 5 mM suramin−0.5 mM PGK are contributions from both free and bound suramin species while the cross peaks of 0.5 mM suramin−10 μM PGK arise from the bound form only due to the cancellation condition reached for 0.5 mM free suramin.

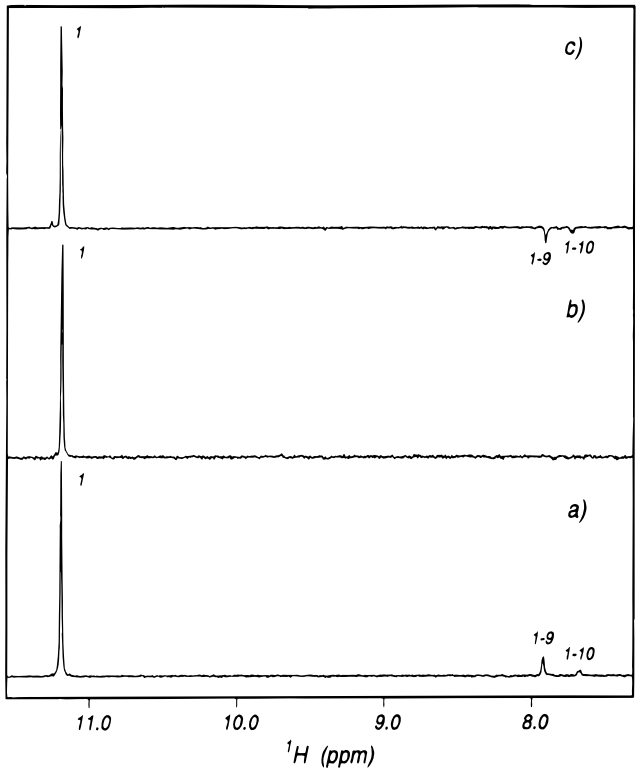

FIGURE 7: One-dimensional traces (selected with D1, the indirect frequency, at the value 11.3 ppm for displaying correlations with amide 1) display correlations to aromatic protons 9 and 10 of the adjacent ring. These are presented for the following spectra: (a) NOESY spectrum of 5 mM suramin, (b) NOESY spectrum of 0.5 mM suramin, (c) ROESY spectrum of 0.5 mM suramin. The relative intensities of peaks 9 and 10 are similar on both 0.5 mM ROESY and 5 mM NOESY spectra. The result confirms that the conformation of the free molecule is not changed with concentration.

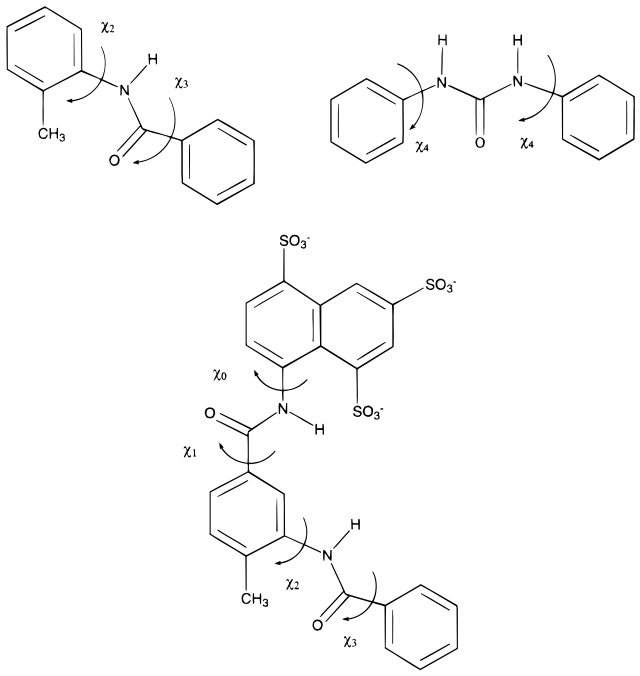

FIGURE 8: Molecular fragments of suramin for which the calculations of energies as functions of dihedral angles have been performed using MACROMODEL.

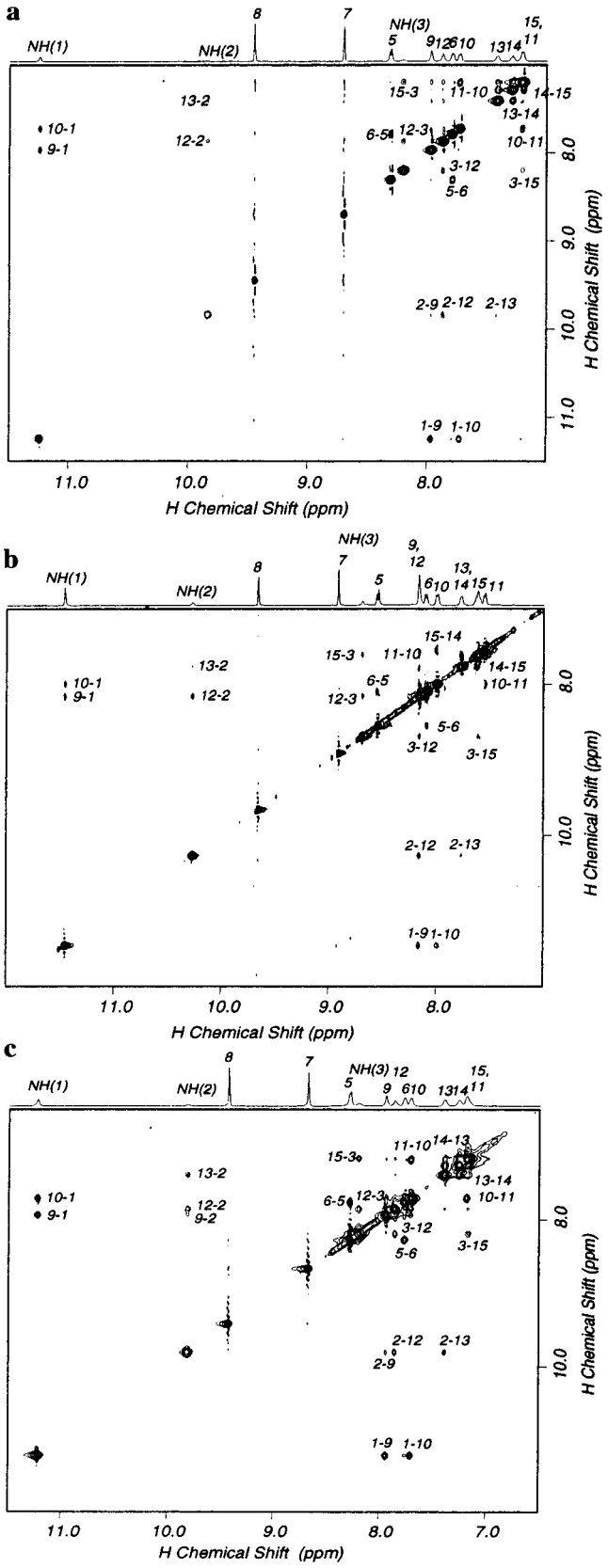

FIGURE 9: Transferred NOESY spectra of (a) 5 mM suramin and 0.5 mM PGK *T. brucei*, (b) 0.5 mM suramin and 10 μM PGK *T. brucei*, (c) 5 mM suramin and 0.5 μM yeast PGK. All samples were in 50 mM d_{11}-Tris buffer containing 100 mM NaCl at pH 6.2 (5 mM suramin) and 5.6 (0.5 mM suramin). The mixing time is 100 ms.

A qualitative difference between the NOESY spectra of the free suramin and transferred NOESY spectra of suramin

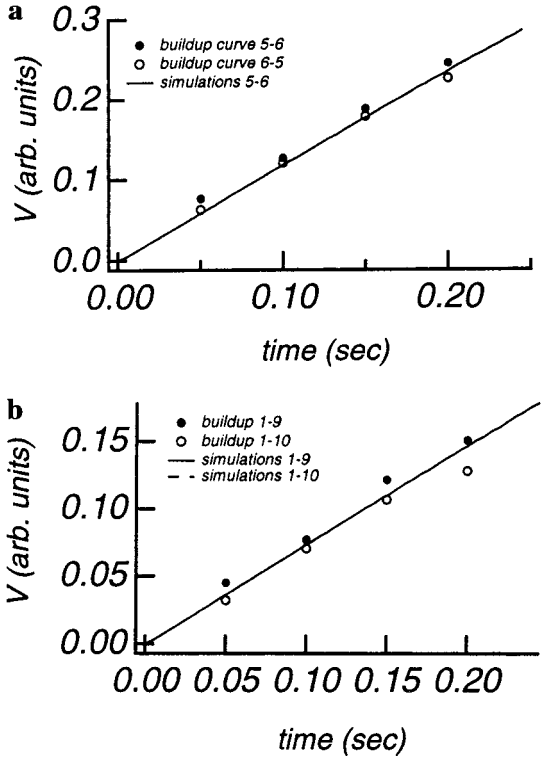

FIGURE 10: Experimental and simulated transferred NOESY buildup curves for 5 mM suramin and 0.5 mM PGK *T. brucei* indicating the normalized cross peak volume vs mixing time for the following pairs of protons: (a) aromatic pairs of protons (calibration peaks) 5−6, (b) amide-to-aromatic proton pairs 1−9 and 1−10.

complexed with PGK is a change in relative intensities of cross peaks between amide 1 and aromatic protons 9 and 10. The relative intensities of the cross peaks between 1 and 10 increased in all three cases measured, and this can be attributed to an increased amount of the conformer II (Table 3) upon binding.

Transferred NOESY Buildup Curves. Transferred NOESY buildup curves for calibration pair of protons 5−6 and amide-to-aromatic pairs of protons (1−9 and 1−10) of 5 mM suramin−0.5 mM PGK *T. brucei*, 0.5 mM suramin−10 μM PGK *T. brucei* and 5 mM suramin−0.5 mM yeast PGK are presented in Figures 10a,b, 11a,b, and 12a,b, respectively. The binding constants of suramin to both yeast and trypanosomal PGK are weak, 167 and 8 μM, respectively, and would suggest fast binding and release (k_{off} greater than 500 s^{-1}) with diffusion-limited on-kinetics. Despite this fact, the buildup curves are not consistent with a fast limit model. In the case of trypanosomal PGK, the fast exchange approximation predicts cross-relaxation rates for the bound suramin that would be very weak regardless of the assumptions about aggregation of the enzyme or about variation of the dissociation constant; the experimental data show much more substantial tNOE intensities. In the case of yeast PGK transferred NOE's exhibit lag periods, i.e., do not build up promptly from zero mixing time. The lag periods cannot be accounted for assuming fast-exchange binding and release. This kind of behavior was observed by us also for transferred NOESY buildup curves of suramin−RNaseH complexes (to be reported elsewhere) and by Kohda et al. (1987) for L-isoleucine and L-valine bound to *E. coli* isoleucyl-tRNA synthetase. The curves have been simulated by computing the relaxation-exchange matrices (as described in the Materi-

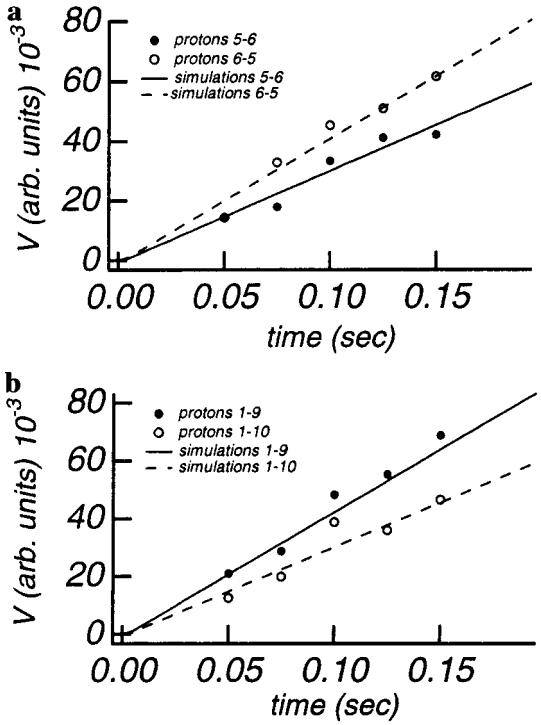

FIGURE 11: Experimental and simulated transferred NOESY buildup curves for 0.5 mM suramin and 10 μM PGK *T. brucei*, indicating the normalized cross peak volume vs mixing time for the following pairs of protons: (a) aromatic pairs of protons (calibration peaks) 5−6, (b) amide-to-aromatic proton pairs 1−9 and 1−10.

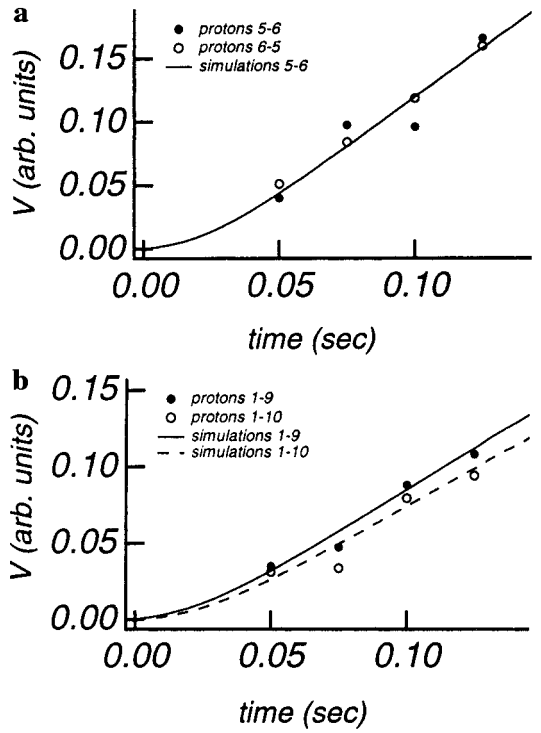

FIGURE 12: Experimental and simulated transferred NOESY buildup curves for 5 mM suramin and 0.5 mM yeast PGK, indicating the normalized cross peak volume vs mixing time for the following pairs of protons: (a) aromatic pairs of protons (calibration peaks) 5−6, (b) amide-to-aromatic proton pairs 1−9 and 1−10.

als and Methods) and the lag phases are attributed to the intermediate exchange behavior. Calculations of the complete relaxation-exchange matrices as a function of mixing time were performed for suramin−PGK complexes.

Simulations of Buildup Curves for Suramin−PGK Complexes: (1) 0.5 mM Suramin−10 μM PGK T. brucei. Buildup curves for the calibration peaks 5−6 and 10−11 were simulated assuming cross-relaxation and self-relaxation rates calculated based on the known interproton distance (2.46 Å) between the adjacent protons on the aromatic rings and correlation times for monomeric PGK (45 kDa, 18 ns) and dimeric PGK (90 kDa, 36 ns); the exchange rates were calculated using diffusion-limited k_{on} rate (10^8 M^{-1} s^{-1}) and the K_d reported (Willson et al., 1993) for suramin bound to PGK *T. brucei* (8 μM). The simulations reproduced experimentally observed buildup curves if k_1 of 67.4 s^{-1} and k_2 of 800 s^{-1} were used. This ratio of kinetic constants is incompatible with the equilibrium calculations outlined in the Materials and Methods section.[2] Use of other binding constants did not result in better simulations. The data can be simulated using an assumption of either monomeric or dimeric enzyme; thus we have no evidence for aggregation of the enzyme under our experimental conditions. The need to use kinetic constants in disagreement with the single step binding equilibrium calculations was seen also in other systems we have studied and is discussed later in terms of a model for binding kinetics.

Exchange rates obtained from simulating the calibration cross peaks (for monomeric PGK) were subsequently used to simulate the buildup curves for the amide-to-aromatic pairs of protons (Figure 10b), and the relaxation rates of the bound suramin were calculated to produce the best fit. The relaxation rates for amide protons are presented in Table 4 along with the corresponding pseudodistances.

(2) 5 mM Suramin−0.5 mM PGK T. brucei. To simulate the buildup curves of 5 mM suramin−0.5 mM PGK *T. brucei*, experimentally measured relaxation rates for each pair of protons of 5 mM free suramin were used in the relaxation-exchange matrix (see Table 1). Calibration peaks were simulated first (vide supra); the exchange rates resulting in the best fit ($k_1 = 221$ s^{-1} and $k_2 = 800$ s^{-1}) were used to simulate the amide-to-aromatic pairs of protons. Experimental and simulated buildup curves are presented in Figure 11a,b; the corresponding relaxation rates and pseudodistances for amide-to-aromatic pairs of protons are given in Table 4.

(3) 5 mM Suramin−0.5 mM Yeast PGK. Suramin is a weaker inhibitor of *yeast* PGK with K_d of 167 μM (Willson et al., 1993). The experimental buildup curves in this case are also impossible to simulate using the experimental exchange rates in one-step equilibrium binding scheme (based on the reported K_d of 167 μM and diffusion-limited k_{on} of 10^8 M^{-1} s^{-1}). As was mentioned above, there are lag phases in the buildup curves, and these imply intermediate exchange rates. These can be simulated by assuming (1) a lower than diffusion-limited apparent value of k_{on} (equivalent to the hypothesis that a lower fraction of free suramin is

[2] For systems with weak binding of the substrate to the receptor, relatively slow transferred NOE buildup rates are expected based on the one-step equilibrium binding scheme with diffusion-limited on-kinetics. In this regime, the apparent rates will be determined by the population-weighted averages of the free and bound cross-relaxation rates, and since the binding is weak, the percent of the substrate bound will never exceed 10% and will depend on the ratio $[L]_T/[E]_T$). If apparent transferred NOE buildup rates are fast, of the order of the cross-relaxation rates expected for the enzyme, the data may already imply that more complex binding kinetics take place. We observed this kind of behavior for the complexes of suramin with yeast PGK and RNaseH.

Table 4: Proton Cross-Relaxation Rates, σ_{ij}, and Pseudodistances, r_{ij}, for Amide-to-Aromatic Proton Pairs of Suramin Complexed with PGK, Calculated by Simulation Using a Full Relaxation Matrix Treatment and Using Kinetic Constants Derived from Simulation of Calibration Cross Peaks (Table 6)[a]

	5 mM suramin−0.5 mM PGK *T. brucei*		0.5 mM suramin−10 μM PGK *T. brucei*		5 mM suramin−0.5 mM PGK *yeast*	
proton pairs	cross-relaxation rate (from tr-NOESY)	pseudodistance, Å	cross-relaxation rate (from tr-NOESY)	pseudodistance, Å	cross-relaxation rate (from tr-NOESY)	pseudodistance, Å
1−9	−4.9	2.2	−6.2	2.1	−2.9	2.4
9−1	−2.1	2.5	−6.2	2.1	−2.9	2.4
1−10	−2.9	2.4	−4.6	2.2	−3.6	2.3
10−1	−4.7	2.2	−4.6	2.2	−3.6	2.3
2−12	−1.2	2.8	−5.5	2.1	−2.1	2.5
12−2	−1.2	2.8	−5.5	2.1	−2.1	2.5
2−13	−0.1	4.15	−4.0	2.2	−2.5	2.6
13−2	−0.48	3.2	−4.0	2.2	−2.5	2.6
2−4	−0.032	5.0	−0.9	2.9	−0.55	3.1
4−2			−0.9	2.9	−0.55	3.1
3−12	−0.77	3.0	−3.8	2.3	−2.7	2.4
12−3	−0.77	3.0	−3.8	2.3	−2.7	2.4
3−15	−4.6	2.2	−2.4	2.4	−1.0	2.8
15−3	−4.6	2.2	−2.4	2.4	−1.0	2.8

[a] The relaxation rates reflect more than one bound conformation. Comparison with the data on free suramin indicates a distinct and reproducible difference in the relative strengths of the 1−9 and 1−10 cross-relaxation rates, namely an increased population of conformer II in Table 3. Other degrees of freedom exhibit subtle differences that are discussed in the text and may be within experimental error.

Table 5: Carbon Spin−Spin Relaxation Rates for 5 mM Suramin, Measured from HSQC-Detected Experiments[a]

carbon no.	K_0	K_1	K_2 ($1/T_2$)	χ^2
5	−0.0040	1.0041	8.12	0.0299
6	0.0046	1.0144	9.78	0.0208
7	−0.0014	0.9741	7.18	0.0077
8	−0.0024	1.0214	8.63	0.0109
9	0.0070	0.9508	30.09	0.0118
10	−0.0057	1.0144	12.55	0.0146
11	0.0102	0.9284	21.22	0.0231
12	0.0049	1.0084	15.12	0.0247
13	−0.0070	1.0068	15.33	0.0235
14	0.0014	0.9841	9.59	0.0132
15	0.0070	0.9484	9.29	0.0137

[a] The data were fit to a single exponential, $I(t)/I(0) = K_0 + K_1 \exp(-K_2 t)$; note that $K_0 \approx 0$ and $K_1 \approx 1$ in every case as expected, and K_2 represents the carbon relaxation rate, R_2.

Table 6: Kinetic Constants for Suramin Bound to the Phosphoglycerate Kinases Obtained by Simulating Transferred NOE's Based on the Equilibrium Binding Model, Where k_{on} Is Assumed To Be Nearly Diffusion-Limited (10^8 M^{-1} s^{-1})[a]

		k_1, s^{-1}		k_2, s^{-1}	
system	K_d, μM	calc: exact (approx)	simulated t-NOE	calc: exact	from simul of the tr-NOE data
0.5 mM suramin + 10 μM PGK *Tb.*	8	16 (16)	67.4	800	800
5 mM suramin + 0.5 mM PGK *Tb.*	8	88 (80)	221	800	800
5 mM suramin + 0.5 mM PGK yeast	167	1782 (1670)	17.6	16700	50.1

[a] See Materials and Methods section for details. The values calculated from simple equilibrium binding are in distinct disagreement with the experimental values.

capable of binding) and (2) complex binding kinetics not well described by a single equilibrium reaction, i.e. $K_d \neq k_2/k_1$ or, alternatively, $k_2/k_1 \neq [L]/[EL(\approx[L]_T/[E]_T)$. The first statement is plausible in view of the multitude of the conformers of free suramin with comparable conformational energy present in equilibrium in solution, while only one or few of them are capable of binding to the enzyme. Therefore, we postulate a lower k_{on} and a more complex binding model than a simple equilibrium binding scheme used to calculate all the exchange rates. An indication of low k_{on} value is also present in suramin−trypanosomal PGK complexes (see above). However, the deviations of the buildup curves from the expected fast-limit kinetics appear to be much more pronounced in the case of the enzymes with weaker binding affinity toward suramin (we also observed the same behavior in suramin−RNaseH complexes—to be reported elsewhere).

Experimental and simulated buildup curves for 5 mM suramin−0.5 mM yeast PGK are shown in Figure 12 (a shows a pair of calibration protons 5−6 and b shows pairs of amide-to-aromatic protons 1−9 and 1−10). Relaxation rates and pseudodistances for amides are presented in Table 4. The exchange rates resulted in the best fit were the following (for monomeric PGK): $k_1 = 11$ s^{-1}, $k_2 = 50$ s^{-1}. Assuming the reported K_d of 167 μM and one-step equilibrium binding scheme this would correspond to $(k_{on})_{app} = 3 \times 10^5$ M^{-1} s^{-1}, $[suramin]_T = 2$ mM; $[PGK]_T = 0.4$ mM.

Discriminating between Different Kinetic Models That May Account for Observed Rate Constants. There are large discrepancies between the rates calculated from the experimental set of parameters such as the known K_d's and the total concentrations of enzymes and suramin, and those used for simulating the buildup curves to produce the best fit; both sets of rate constants are given in Table 6. Both k_1 and k_2 are low by 1−2 orders of magnitude in the case of yeast PGK. Apparently a small fraction of suramin is binding, and therefore, the **apparent** value for k_{on} is low by orders of magnitude. Secondly, the **ratio** of k_1 to k_2 cannot be simulated. This ratio is approximately independent of all assumptions about K_d and k_{on}, since $k_2 = k_{on}K_d$, $k_1 = k_2([E]_T/[L]_T)$: for the simple binding model it depends only on the stoichiometry $[E]_T/[L]_T$ which is fairly well known. When the ratio, k_1/k_2, is in disagreement with calculations, a different kinetic model must be proposed. More complex binding kinetics is quite likely to take place in suramin−PGK complexes due to multiple suramin conformers in solution and possibly due to electrostatics-governed binding. We considered the following kinetic schemes:

$$\mathbf{E} + \mathbf{2L} \underset{k_{21}}{\overset{k_{11}}{\rightleftharpoons}} \mathbf{EL} + \mathbf{L} \underset{k_{22}}{\overset{k_{12}}{\rightleftharpoons}} \mathbf{EL_2} \qquad (10)$$

$$\mathbf{E} + \mathbf{L} \underset{k_{21}}{\overset{k_{11}}{\rightleftharpoons}} \underset{\substack{\text{nonspecifically bound}\\ \text{inhibited no NOE}\\ \text{(encounter complex)}}}{\mathbf{(EL)^*}} \underset{k_{22}}{\overset{k_{12}}{\rightleftharpoons}} \underset{\substack{\text{specifically}\\ \text{bound inhibited}\\ \text{complex NOE's}}}{\mathbf{EL}} \qquad (11)$$

It is easy to show that the first model, sequential binding of two substrate molecules (10) cannot provide an adequate explanation for the observed behavior. The second model (11), formation of an "encounter complex" (loose electrostatic complex) and its rearrangement into a final stable enzyme-substrate complex, is consistent with the experimental conditions and rate constants obtained from simulations and could be one of the possible mechanisms of forming suramin−PGK complexes.[3] This binding mechanism has been reported or proposed for interactions of various enzymes with their substrates and inhibitors (Schreiber & Fersht, 1993; Sharp et al., 1987; Wallis et al., 1995).

Conformational Analysis of Suramin Bound to Phosphoglycerate Kinases from T. brucei and Yeast. For each of the degrees of freedom of suramin molecule bound to PGK, conformational preferences can be analyzed in a way similar to that for free suramin. As was pointed out above, it is not possible to attribute the observed NOE cross-relaxation rates and resulting pseudodistances to any single conformer in a half-molecule of suramin. However, if the binding is specific and the bound molecule is in a single preferred conformation, the two halves of it can be treated as separate conformers with the population ratio of 1:1. If the binding is weaker and nonspecific, which is quite plausible for the yeast PGK−suramin complexes, the above assumption is no longer valid. In the case of yeast PGK, complex kinetics of binding result in uncertainties in the calculated relaxation rates, and the interpretation of the transferred NOE data and the derived bound state conformation are ambiguous.

(1) Conformational Analysis of Suramin Bound to Trypanosomal PGK. Under the assumption of a 1:1 population ratio between the two conformers (each belonging to a half-molecule), one can analyze the pseudodistances and find the corresponding dihedral angles. The dihedral angle χ_0 is invariant upon binding since amide proton 1 is strongly hydrogen bonded to the adjacent sulfonate group. Another degree of freedom which does not change upon binding is the dihedral angle χ_2. As for free suramin, very weak NOE's are observed for 4−2 and 9−2 suggesting that this degree of freedom is highly nonplanar (due to strong steric clashes of the amide proton with the methyl group on the aromatic ring, in agreement with MACROMODEL calculations). These two degrees of freedom form a special case in a sense of being fixed in the same conformation for both halves of the molecule; the rest of the degrees of freedom are not forced into a single conformer, and the corresponding dihedrals (χ_1, χ_3, and χ_4) take different values for each half of the molecule (discussed below).

For the degree of freedom around χ_1, NMR data indicate that each of the two limiting conformers I and II in Table 3 is out-of-plane to a similar extent. The calculated distance of 2.1−2.2 Å corresponds to a dihedral angle of 26−34° which is slightly less out-of-plane than in the free suramin.

For dihedral angle χ_3 the data for 5 mM suramin−0.5 mM PGK and 0.5 mM suramin−10 μM PGK give different estimates. The data for 5 mM suramin suggest χ_3 to be around 60° (2.7−2.8 Å) for conformer III and 75° (3.2 Å) for conformer IV. For 0.5 mM suramin the calculated distances are shorter (2.1−2.3 Å for both conformers III and IV) with the corresponding dihedral angles of 32−36°. A possible explanation would be faster exchange with the solvent in the 5 mM sample resulting in diminishing intensities of the amide peaks and, therefore, longer apparent distances and larger dihedrals. This explanation is consistent with the fact that for amide proton 1 NOE intensities and relaxation rates are similar in both 5 and 0.5 mM suramin, and this amide proton has a much slower exchange rate with the solvent. There may be also larger errors associated with calculated distances in the 5 mM suramin due to nonvanishing contributions to the NOE cross peaks from the free form. Therefore, we think that shorter distances and smaller dihedrals better describe the molecule.

For χ_4, represented by conformers V and VI, the data indicate distances of 2.3−2.5 Å corresponding to a near-planar arrangement. This result differs significantly from the free suramin molecule where χ_4 is about 50° out-of-plane.

Since the degrees of freedom of suramin are independent of one another, there are 2^8 possible bound conformers of suramin; those are indistinguishable on the basis of the NMR data.

(2) Conformational Analysis of Suramin Bound to Yeast PGK. Since nonspecific binding is likely for suramin−yeast PGK complexes, the conformation of suramin bound to the yeast enzyme derived based on the transferred NOESY data could contain large errors for each degree of freedom. The main objective of analyzing this case was to compare it to the suramin−trypanosomal PGK complexes for the purpose of designing lead compounds that would be targeted specifically against the trypanosomal PGK. In the following discussion we will nevertheless treat the data assuming specific binding and 1:1 population ratio between the conformers in each half-molecule, for simplicity.

According to the transferred NOESY data, there are certain changes associated with each of the degrees of freedom for suramin bound to yeast PGK as compared to both free suramin and suramin bound to PGK from *T. brucei*. Dihedral angle χ_1 for both conformers I and II appears to be 36−40° (distances of 2.3−2.4 Å) which is similar to the free suramin (35°). Dihedral angle χ_2 is again invariant upon binding, and this fragment of the molecule is in a highly nonplanar arrangement. Dihedral angle χ_3 appears to be between 50 and 55° (distances of 2.5−2.6 Å) for both conformers III and IV in Table 3. This is slightly larger than in both free (40−45°) and bound to the *T. brucei* PGK suramin (32−36°). Dihedral angle χ_4 is about 180° (2.4 Å) for conformer V and 60° (2.8 Å) for conformer VI. In free suramin this dihedral was about 30° for both conformers, and in suramin bound to trypanosomal PGK for both V and VI, it was 180°. These differences in derived distances and dihedral angles are subject to intrinsic experimental errors.

[3] A set of solutions for the rate constants consistent with experimental data for suramin−PGK complexes was obtained under the condition that k_{11} is fast (diffusion-limited), k_{12} and k_{21} have a consistent set of solutions but were chosen so that k_{22}, which is the apparent k_{off} and is determined by the transferred NOESY analysis of the calibration pairs of protons, in the simulations is consistent with the apparent value for the K_d.

CONCLUSIONS

At room temperature and 5 mM concentration, suramin is a multimeric complex of approximately five molecules, while at 0.5 mM suramin is a monomer. The NMR data suggest rapid averaging between a large number of conformations. Each degree of freedom has been separately analyzed, and it has been shown that while some of them are essentially locked, others have very weak preferences between two conformers, both exhibiting nonplanar arrangement of the rings relative to the adjacent amides. While the degree of nonplanarity was anticipated by molecular modeling, the detailed preferences were not. As a result of the very large number of degrees of freedom, locking suramin into a unique and bioactive conformer could potentially reduce the binding constant from the micro- to the nanomolar regime.

Transferred NOE data indicate strong magnetization exchange associated with the bound form. The absolute rates are inconsistent with a simple one-step binding mechanism but consistent with formation of an electrostatic encounter complex before binding.

Changes in conformation of suramin upon binding to phosphoglycerate kinases from *S. cerevisae* and *T. brucei* were detected. Binding results in locking the suramin molecule into a specific conformer, and it appears to be asymmetric (with respect to each half-molecule) in both cases. Since all degrees of freedom in the suramin molecule are independent of one another, there are still 2^8 possible ways to construct the bound conformation of the molecule, and those are indistinguishable on the basis of solution NMR data.

ACKNOWLEDGMENT

The authors would like to thank Dr. Guy Lippens and Dr. Klass Hallenga (ULB, Brussels, Belgium) and Dr. Fred Opperdoes and Dr. Paul Michels (UCL, Brussels, Belgium) for extensive support and advice in the initial stages of this research. The authors would also like to thank Dr. Craig Bingman (Columbia University) for his help with light-scattering experiments.

REFERENCES

Borchert, T. A., Pratt, K., Zeelen, J. P., Callens, M., Noble, M. E. M., Opperdoes, F. R., Michels, P. M., & Wierenga, R. K. (1992) *Eur. J. Biochem. 211*, 703−710.

Boyle, H. A., Fairbrother, W. J., & Williams, R. J. P. (1989) *Eur. J. Biochem. 184*, 535−543.

Brisson, J., & Brissé, F. (1985) *Can. J. Chem 63*, 3390−3397.

Campbell, A. P., & Sykes, B. D. (1993) *Annu. Rev. Biophys. Biomol. Struct. 22*, 99−122.

Carr, H. Y., & Purcell, E. M. (1954) *Phys. Rev. 94*, 630−638.

Clanton, D. J., Moran, R. A., McMahon, J. B., Weislow, O. S., Buckheit, R. W., Hollingshead, M. G., Ciminale, V., Felber, B. K., Pavlakis, G. N., & Bader, J. P. (1992) *AIDS 5*, 771−781.

Collins, J. M., Klecker, R. W., Yarchoan, R., Lane, H. C., Fauci, A. S., Redfield, R. R., Broder, S., & Myers, C. E. (1986) *J. Clin. Pharmacol. 26*, 22−26.

Fairlamb, A. H., & Bowman, I. B. R. (1980) *Mol. Biochem. Parasitol. 1*, 315−333.

Farrow, N. A., Muhandiram, R., Singer, A. U., Pascal, S. M., Kay, C. M., Gish, G., Shoelson, S. E., Pawson, T., Forman-Kay, J. D., & Kay, L. E. (1994) *Biochemistry 33*, 5984−6003.

Fourneau, V., Tréfouel, J., & Vallée, J. (1924) *Ann. Inst. Pasteur 38*, 81.

Ganis, P., Avitabile, G., Migdal, S., & Goodman, M. (1971) *J. Am. Chem. Soc. 93*, 3328−3331.

Goeddel, D. V. (1990) *Gene expression technology*, Academic Press, San Diego.

Hammes, G. G., & Schimmel, P. R. (1970) in *Enzymes* (Boyer, P. D., Eds.) pp 109, Academic Press, New York.

Harte, D. (1990) *Parasitology Today 5*, 117−120.

Ishima, R., & Nagayama, K. (1995) *Biochemistry 34*, 3162−3171.

Jentsch, K., Hunsmann, G., Hartmann, H., & Nickel, P. (1987) *J. Gen. Virol. 68*, 2183−2192.

Kashino, S., Ito, K., & Haisa, M. (1979) *Bull. Chem. Soc. Jpn. 52*, 365−369.

Kohda, D., Kawai, G., Yokoyama, S., Kawakami, M., Mizushima, S., & Miyazawa, T. (1987) *Biochemistry 26*, 6531−6538.

Landy, S. B., & Rao, B. D. N. (1989) *J. Magn. Reson. 81*, 371−377.

Lee, W., & Krishna, N. R. (1992) *J. Magn. Reson. 98*, 36−48.

Lipari, G., & Szabo, A. (1980) *Biophys. J. 30*, 489−506.

Lipari, G., & Szabo, A. (1982a) *J. Am. Chem. Soc. 104*, 4546−4559.

Lipari, G., & Szabo, A. (1982b) *J. Am. Chem. Soc. 104*, 4559−4570.

Lippens, G., Dhalluin, C., & Wieruszeski, J.-M. (1995) *J. Biomol. NMR 5*, 327.

Lippens, G. M., Cerf, C., & Hallenga, K. (1992) *J. Magn. Reson. 99*, 268−281.

Macura, S., & Ernst, R. R. (1980) *Mol. Phys. 41*, 95−117.

Marion, D., & Wüthrich, K. (1983) *Biochem. Biophys. Res. Commun. 113*, 967−974.

Meiboom, S., & Gill, D. (1958) *Rev. Sci. Instrum. 29*, 688−691.

Middaugh, C. R., Mach, H., Burke, C. J., Volkin, D. B., Dabora, J. M., Tsai, P. K., Bruner, M. W., Ryan, J. A., & Marfia, K. E. (1992) *Biochemistry 31*, 9016−9024.

Misset, O., & Opperdoes, F. R. (1987) *Eur. J. Biochem. 162*, 493−500.

Mohan, P. (1993) *Drug Dev. Res. 29*, 1−17.

Ni, F. (1994) *Progr. NMR Spectr. 26*, 517−606.

Nickel, V. P., Haack, H.-J., Widjaja, H., Ardanuy, U., Gurgel, C., Düwel, D., Loewe, H., & Raether, W. (1986) *Arzneim.-Forsch./ Drug Res. 36 (II)*, 1153−1157.

Opperdoes, F. (1987) *Annu. Rev. Microbiol. 41*, 127−151.

Otting, G., Grutter, R., Leupin, W., Minganti, C., Ganesh, K. N., Sproat, B. S., Gait, M. J., & Wüthrich, K. (1987) *Eur. J. Biochem. 166*, 215−220.

Palmer, A., Rance, M., & Wright, P. (1991) *J. Am. Chem. Soc. 113*, 4371−4380.

Palmer, A. G., III, Hochstrasser, R. A., Millar, D. P., Rance, M., & Wright, P. E. (1993) *J. Am. Chem. Soc. 115*, 6333−6345.

Palmer, A. G., III, Williams, J., & McDermott, A. (1996) *J. Phys. Chem. 100*, 13293−13310.

Peng, J. W., & Wagner, G. (1992a) *Biochemistry 31*, 8571−8586.

Peng, J. W., & Wagner, G. (1992b) *J. Magn. Reson. 98*, 308−332.

Piotto, M., Saudek, V., & Sklenár, V. (1992) *J-Bio NMR 2*, 661−665.

Polenova, T. (1997) in Conformational Analysis of Pharmaceutical Suramin Free and in the Presence of Its Target Receptors by Solution NMR: What We Learned from and about Transferred NOESY, Ph.D. Thesis, Columbia University, New York, 341 pp.

Schreiber, G., & Fersht, A. R. (1993) *Biochemistry 32*, 5145−5150.

Schurr, J. M., Babcock, H. P., & Fujimoto, B. S. (1994) *J. Magn. Reson., Ser. B 105*, 211−224.

Shaka, A. J., Keeler, J., & Freeman, R. (1983) *J. Magn. Reson. 52*, 335−338.

Sharp, K., Fine, R., & Honig, B. (1987) *Science 236*, 1460−1463.

Sklenár, V., Piotto, M., Leppik, R., & Saudek, V. (1993) *J. Magn. Reson. 102*, 241−245.

Stein, C. (1993) *Cancer Res. 53*, 2239−2248.

Vansterkenburg, E., Coppens, I., Wilting, J., Bos, O., Fischer, M., Janssen, L., & Opperdoes, F. (1993) *Acta Tropica 54*, 237−250.

Wallis, R., Moore, G. R., James, R., & Kleanthous, C. (1995) *Biochemistry 34*, 13743−13750.

Willson, M., Callens, M., Kuntz, D. A., Perié, J., & Opperdoes, F. R. (1993) *Mol. Biochem. Parasitol. 59*, 201−210.

BI970297M